MDPI

Article

Characteristics and Reservoir Development Model of the Unconformity Caused by Huaiyuan Movement in Bohai Bay Basin, China: A Case Study of Chengdao-Zhuanghai Buried Hill in Jiyang Depression

Ruijuan Liu [1,2], Guozhi Wang [3,4,*], Yongshi Wang [5], Xuefeng Hao [2], Feng Qin [2], Xianxu Fang [6], Wei Meng [2] and Gang Liu [1]

[1] Colleges of Earth Sciences, Chengdu University of Technology, Chengdu 610059, China; liuruijuan2004@126.com (R.L.)
[2] Research Institute of Petroleum Exploration and Development, Shengli Oilfield, SINOPEC, Dongying 25700, China
[3] National Key Laboratory of Oil and Gas Reservoir Geology and Exploitation, Chengdu University of Technology, Chengdu 610059, China
[4] Institute of Sedimentary Geology, Chengdu University of Technology, Chengdu 610059, China
[5] Sinopec Shengli Oilfield Company, Dongying 25700, China; wangysh623@sina.com
[6] School of Geosciences, China University of Petroleum (East China), Qingdao 266580, China
[*] Correspondence: wangguozhi66@163.com; Tel.: +86-133-8817-8798

Abstract: It is beneficial in terms of the theoretical significance and application prospects to define the structure and reservoir development model of the lower Paleozoic unconformity in the Jiyang Depression of Bohai Bay Basin, China, for oil and gas exploration of unconformity in carbonate strata. Geological and geochemical evidence shows that a regional unconformity formed during the Huaiyuan Movement in the lower Paleozoic strata of the Jiyang Depression. Along the top of the regional unconformity between the Yeli Liangjiashan Formation and Fengshan Formation, various types of karst breccia have developed, showing prominent characteristics of development and vertical karst zonation. The paleokarst zone can be divided into the vadose zone and the underflow zone, and there are apparent differences between the two zones in terms of the mode of karst activity and type of reservoir space. Primitive sedimentary microfacies, dolomitization, and supergene karstification controlled the reservoirs of the Fengshan Formation and Yeli-Liangjiashan Formation. There are significant differences in the original physical properties due to the differences in the original sedimentary microfacies. The pore development of granular dolomite of high-energy beach facies has the best reservoir performance. In the later period, the superposition of dolomitization and supergene karstification resulted in apparent differences in karst development mode, development intensity, reservoir type, and reservoir physical properties. Among them, the granular dolomite reservoir has the best physical properties and has developed a cavity-type reservoir that has a planar distribution along an unconformity surface.

Keywords: Chengdao-Zhuanghai buried hill; the lower Paleozoic; Huaiyuan movement; unconformity structure; supergene karstification; reservoir development model

1. Introduction

Statistics show that nearly one-third of the world's large carbonate oil and gas fields are related to unconformities [1–3]. Previous studies have shown that due to the influence of tectonic movement, carbonate strata are exposed to the surface, and under the influence of atmospheric freshwater leaching, supergene karstification occurs to form unconformity, and a large number of dissolution pores and caves that are developed inside the unconformity can be used as good reservoirs and essential channels for oil and gas migration [4–13].

Therefore, this critical study predicts the distribution of oil and gas reservoirs in carbonate strata to clarify the characteristics and development model of unconformity. Different scholars have effectively identified unconformity interfaces from the perspective of stratigraphic cycles, C and O isotopes, trace element data, and foraminiferal biostratigraphy [14–20]. On this basis, the karst profile structure and horizontal distribution controlled by paleokarst under the unconformity have been deeply analyzed by combining present and past methods. The zonation and intensity of karst vertically and horizontally in carbonate reservoirs with unconformities are vital factors controlling the formation and distribution of secondary reservoir spaces [17,21–27].

The lower Paleozoic strata in the Jiyang Depression of Bohai Bay Basin, China, experienced multiple stages of tectonic uplift, weathering and leaching, and hydrothermal transformation; these activities occurred in the Huaiyuan Movement (early Caledonian Movement), late Caledonian Movement, early Hercynian Movement, Indosinian Movement, Yanshan Movement, and Himalayan Movement [26]. The early Alpine stage, mainly the Mesozoic, is called the Yanshan Stage in China. The narrow Alpine Age, called the "Himalayan Age" in Asia, happened in the Cenozoic. Theoretically, there may be multistage unconformities and multiple zones of karst reservoirs. Previous studies have focused mainly on Himalayan unconformities and paleokarstification [28,29]. Although some petroleum geologists have proposed that the Huaiyuan Movement affected the Jiyang Depression [30], they believe that the reservoirs under the tectonic surface were not affected or controlled by supergenetic activities during the Huaiyuan Movement but rather by multistage uplift and dissolution that affected the surficial lake environment in the Paleogene faulted basin [26,31]. In addition to the lack of direct geological and geochemical evidence, the record of the Huaiyuan Movement has been a controversial and unresolved issue. With the continuous increase in oil and gas exploration in buried hills in the Jiyang Depression, the discovery of large-scale oil reservoirs in the Yeli Formation and Liangjiashan Formation, and the accumulation of a large amount of drilling data, petroleum geologists have begun to understand the Huaiyuan Movement.

The Huaiyuan Movement, first named by Li Siguang (1939) [32], is an important regional and multistage "curtain" tectonic movement that occurred in the early Paleozoic on the North China platform; the movement lasted from the end of the Zhangxia Stage in the middle Cambrian to the Liangjiashan Stage in the Early Ordovician. Frequently exposed strata between the Majiagou Formation and the Liangjiashan Formation and within the Yeli and Liangjiashan Formations were denuded from the Cambrian to the Ordovician. The unconformity between the late Liangjiashan and Majiagou stages is the prominent unconformity formed by this movement, and the duration of this depositional discontinuity is 3~18 Ma [32,33]. The Jiyang Depression is one of the essential oil-bearing basins on the North China Platform, and the whole tectonic evolution of the Huaiyuan Movement had an essential influence on the formation of the lower Paleozoic reservoir and oil and gas migration and accumulation in the Jiyang Depression. At present, because the duration of exposure and denudation in this period was shorter than that during the Caledonian Movement, the evidence of the record of this movement is relatively hidden, and it has not attracted extensive or in-depth attention from geologists [30,31]. What are the characteristics of the Huaiyuan Movement in the Jiyang Depression? Did it control the reservoir? Is this reservoir widely developed throughout the depression? What are the development patterns of the reservoir? All of these questions need to be answered. Therefore, the lower Paleozoic Chengdao-Zhuanghai buried hill in the Jiyang Depression is selected as the research area. Through field outcrop surveys, core observations, hand sample observations, geochemical analyses, and seismic and drilling data, evidence of unconformities, the characteristics of the development of unconformity structures, and reservoir development models during the Huaiyuan Movement are revealed. This study provides a new direction for research on lower Paleozoic reservoir prediction in the Jiyang Depression. It significantly contributes to the study of unconformity in carbonate strata worldwide.

2. Geological Background

The Chengdao-Zhuanghai buried hill is located to the northeast of the Jiyang Depression in the Bohai Bay Basin, eastern China (Figure 1). It is located in the central and eastern parts of the North China Platform, adjacent to three hydrocarbon-generating depressions (Huanghe Kou Sag, Bozhong Sag, and Chengbei Sag) on three sides, and connected to the Chengbei Sag on the southwest, the Bozhong Sag on the northeast, and the Huanghe Kou Sag on the east. The oil source conditions are excellent (Figure 2a).

The multi-stage tectonic movement influenced the formation of the Chengdao-Zhuanghai buried hill. During the Caledonian tectonic movement, the Lower Paleozoic carbonate platform as a whole was compressed and uplifted, the strata suffered denudation, and the Upper Ordovician series, Silurian Series, Devonian series, and Lower Carboniferous Series were missing, forming sedimentary discontinuities as long as 120 Ma. In the Hercynian tectonic movement stage, the Upper Paleozoic strata developed the cratonic sedimentary stage of land–sea intersection. In the late period, the whole was uplifted to land, suffered denudation, and the tectonic activity was quiet, and the fault was not developed. During the Indosinian tectonic movement, the early and Middle Triassic were stable deposits, while the NE–SW compression uplift and denudation occurred in the late Triassic. In the stage of Yanshan tectonic movement, the early to Middle Jurassic was in the process of filling and replenishing with weak fault activity, and the Late Jurassic experienced overall uplift, the Early Cretaceous NE–SW extensional fault depression, and the Late Cretaceous compressive uplift and strata denudation. In the stage of the Xishan tectonic movement, the S–N intense extensional fault depression occurred in the Paleogene, and the depression settlement occurred from the Neogene to the Quaternary, and the late sediments overlay the earlier sedimentary strata, forming the present buried hill [34].

Chengdao-Zhuanghai buried hill developed from the bottom up: Archean, Lower Paleozoic Cambrian, Ordovician, Upper Paleozoic Carboniferous, Permian, Mesozoic Jurassic and Cretaceous. The lower Paleozoic strata of the Chengdao-Zhuanghai buried hill are Cambrian and Ordovician in age (Figure 2b), formed in a marine environment, and are a set of stable carbonate strata. Influenced by the uplift and denudation of the Caledonian Movement, Hercynian Movement, Indosinian Movement, Yanshan Movement, Himalayan Movement, and other tectonic movements in the study area, the transformation and destruction of supergenetic karstification in multiple stages occurred, forming multistage unconformities and multiple paleokarst interfaces (Wang et al. [35]). In different parts of the Chengdao-Zhuanghai buried hill, parallel unconformities in the Cenozoic, Mesozoic, or some of the upper Paleozoic strata cover the lower Paleozoic Badou Formation, Majiagou Formation, or Yeli-Liangjiashan Formation. The late Cambrian and Ordovician strata were mainly affected by the Huaiyuan Movement (early Caledonian Movement), the late Caledonian Movement–early Hercynian Movement, and the Indosinian Movement, while the Yanshan Movement and the Himalayan Movement had relatively weak influences on the lower Paleozoic strata. Current exploration practices have shown that there are good reservoir spaces and migration channels in the lower Paleozoic strata in the Chengdao-Zanghai buried hill, resulting in oil and gas enrichment in several Formations (the Badou Formation, Majiagou Formation, Yeili Liangjiashan Formation, and Fengshan Formation) [35,36].

The lithologies of the Yeli-Liangjiashan Formation in the study area are dominantly dolomitic karst breccia, crystalline dolomite, and granular dolomite. Crystalline limestone, calcareous dolomite, dolomitic limestone, argillaceous dolomite, and mudstone are also present in local areas, with total formation thicknesses of 90~150 m. The Fengshan Formation is mainly composed of dolomitic or calcareous karst breccia, crystalline limestone, and crystalline dolomite, and some areas contain muddy limestone. The total formation thicknesses are 100~110 m. The Majiagou Formation, overlying the Yeli-Liangjiashan Formation, is dominated by limestone and dolomitic limestone interbedded with several sets of micritic dolomite and salt-rich rocks, with thicknesses ranging from 150 to 600 m (Figure 2b) [35]. In terms of sedimentary facies evolution, the Cambrian–Early Ordovician was mainly divided into three stages: the continuous transgression stage from the early Cambrian

Mantou stage to the middle Cambrian Xuzhuang stage, which was dominated by a tidal flat environment; the middle Cambrian Zhangxia to late Cambrian Gushan Changshan stage, during which the maximum extent of the ocean occurred and was dominated by subtidal high-energy shoals (Zhangxia stage), as well as open sea; and the late Fengshanian and Early Ordovician stage, during which the water was shallower, and the Yeli-Liangjiashan and Fengshan Formations formed in tidal flat and restricted sea environments. Granular beach facies, evaporative platform dolomite facies, restricted platform limestone facies, and limestone-dolomite facies are of equal occurrence in the Chengdao-Zhuanghai area in the northeast Jiyang Depression (Figure 3) [26,37].
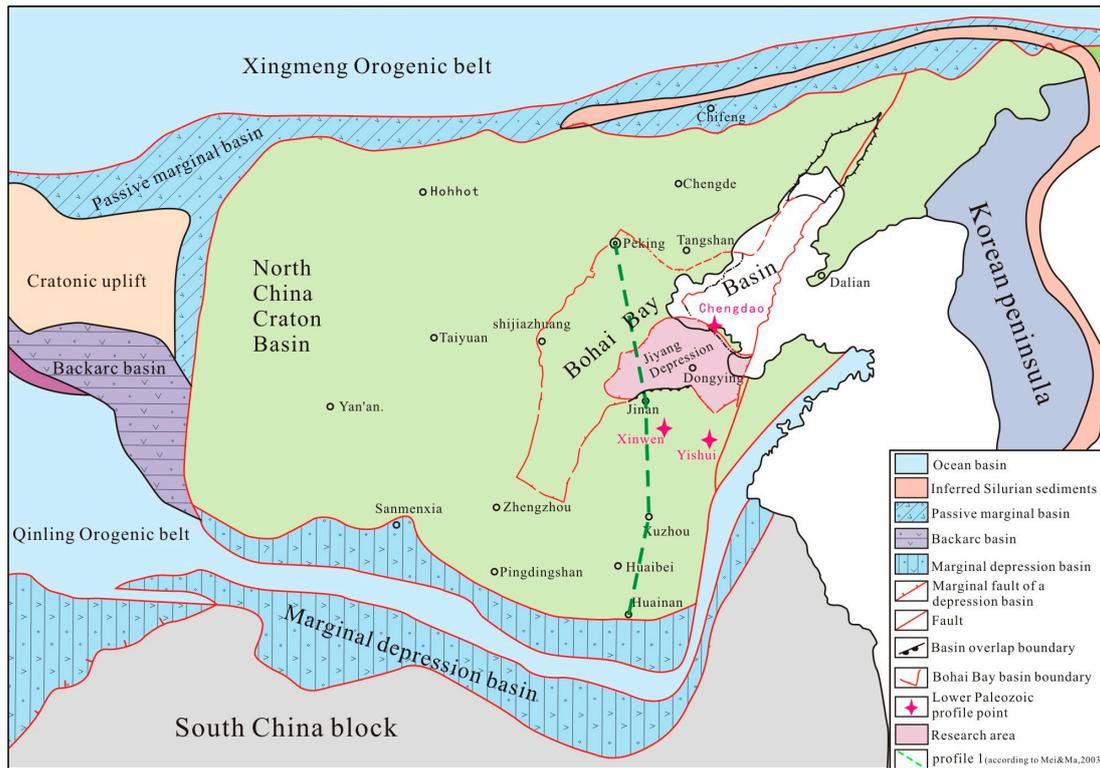

Figure 1. Early Paleozoic tectonic-paleogeography diagram of North China Plate (modified according to Ma Shuai, 2023 [37]).
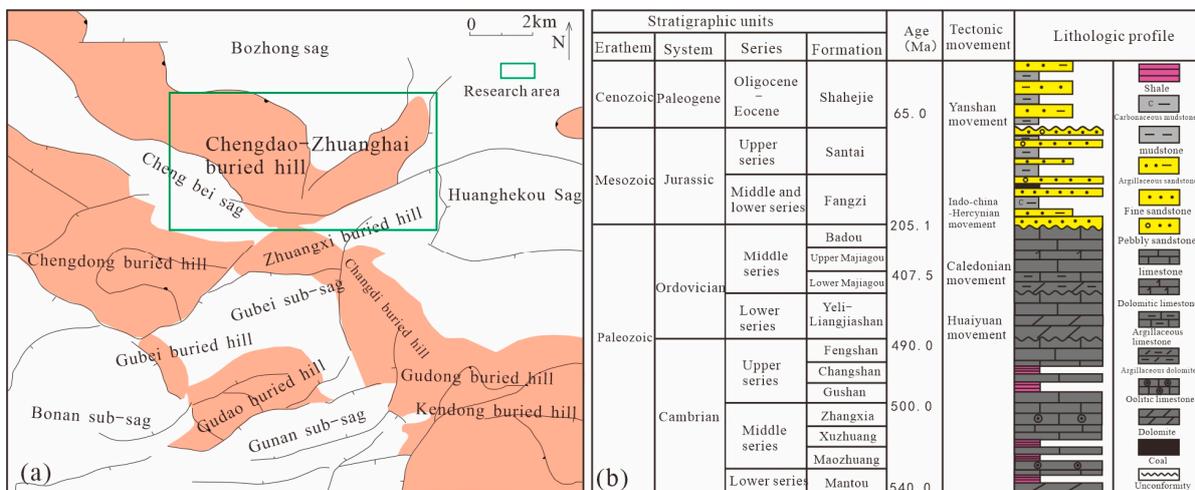

Figure 2. (**a**) Structural location map of Chengdao-Zhuanghai buried hill area. (**b**) Stratigraphic composite column chart of Chengdao-Zhuanghai buried hill (CB302).
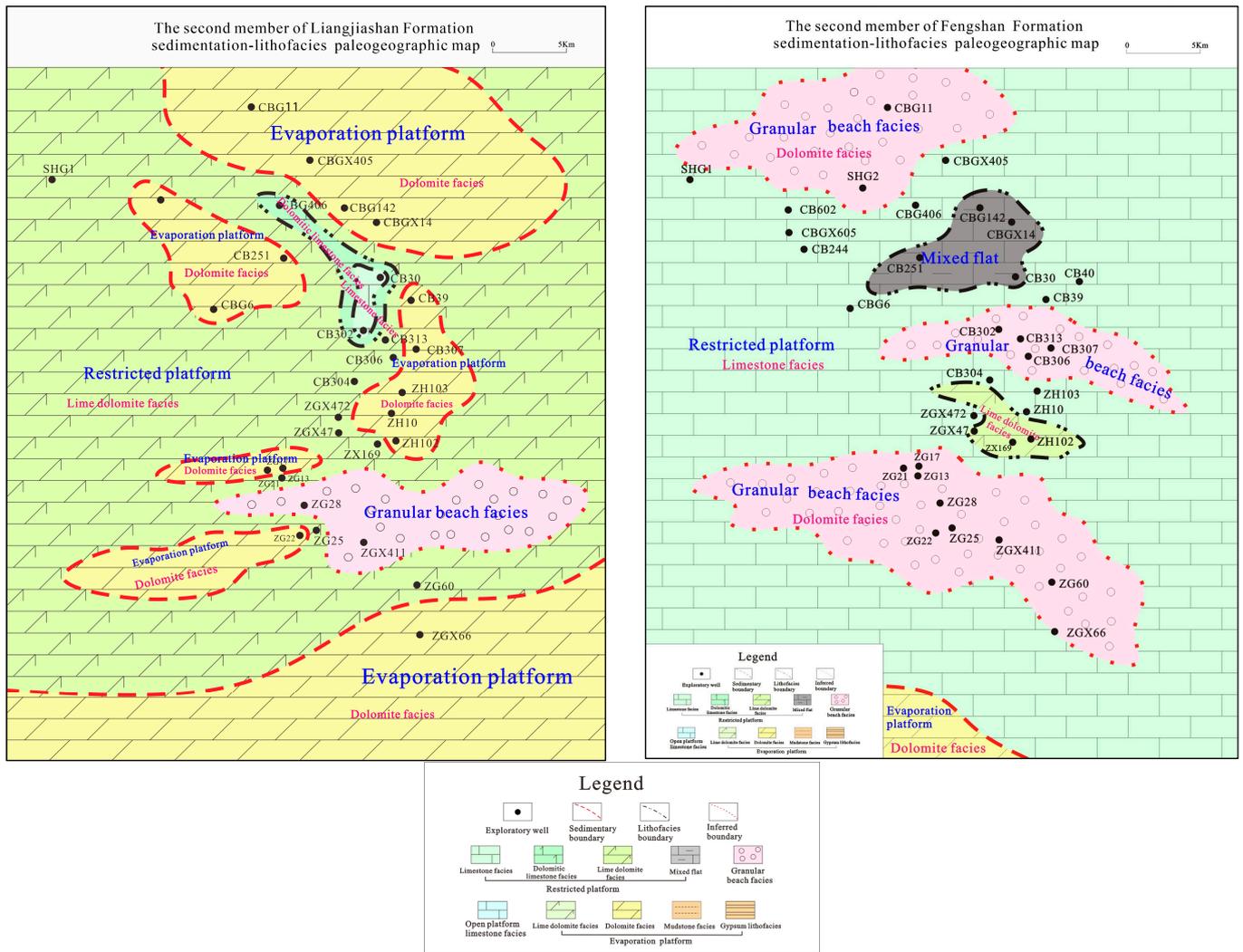
Figure 3. Yeli-Liangjiashan Formation and Fengshan Formation. sedimentation-lithofacies paleogeographic map in Chengdao and Zhuanghai buried hill (according to Sinopec Shengli oilfield, 2022).

3. Materials and Methods

In this study, the evidence, structural characteristics and reservoir development model of unconformities in the Yeli-Liangjiashan Formation and Fengshan Formation are studied by means of outcrop exploration and core observations. Two observation areas, the Xinwen area of Xintai city and the Yishui area of Linyi city, were selected for the field survey. The specific survey sites are shown in Figure 4. The characteristics of lithology, solution holes (pores), and cracks in the outcrop directly show the longitudinal characteristics of an unconformity structure. Cores of 12 wells with a total length of 150 m were selected from the Chengdao-Zhuanghai buried hill for detailed observation. The characteristics of rock types, cracks, and solution holes (pores) in the scale range of hand specimens were obtained. Sixty representative samples were selected from the cores to prepare thin sections. The rock types, reservoir space types, and intercalation characteristics were studied in detail with a ZEISS Imager.A2 m microscope (Carl Zeiss, Oberkochen, Germany). The characteristics of cracks, solution holes (pores), and cementation of karst reservoirs on a microscopic scale were obtained. On this basis, 47 representative samples were selected, and C and O isotopes ($\delta^{13}C_{V\text{-}PDB}$/‰ and $\delta^{18}O_{V\text{-}PDB}$/‰) were analyzed by a MAT253 gas stable isotope mass spectrometer ($\delta^{13}C$, with 0.0037‰ and $\delta^{18}O$, with 0.013‰). Twenty-two pieces of carbon and oxygen isotope analysis data were obtained, and five pieces of carbon

and oxygen isotope analysis data were obtained from literature research to complete the study of fluid types in the paper. Sr isotope analysis ($\delta^{87}Sr_{V\text{-}PDB}/‰$, $\delta^{86}Sr_{V\text{-}PDB}/‰$) of the cement was performed with a MAT261 solid stable isotope mass spectrometer (accuracy $^{87}Sr/^{86}Sr < 10$ ppm). Eighteen sets of analytical data were obtained that could be used to distinguish the period of occurrence of supergene karstification. Core observations and sampling were completed in the core bank at the Shengli Oilfield, and thin-section observations and geochemical analysis were completed at the Academy of Geosciences, Chengdu University of Technology Laboratory.

4. Results

4.1. Peripheral Outcrop Characteristics

The points where the outcrop was observed are located in the Matouya area, Xinwen city, Shandong Province (Area 1), and in the Yangzhuang area, Yishui County, Linyi city, Shandong Province (Area 2), both of which are dominated by the exposed Yeli-Liangjiashan Formation, with a small amount of exposed Fengshan Formation strata. The sedimentary characteristics of the Yeli-Liangjiashan Formation and Fengshan Formation are similar to those of the whole North China Platform in the late Cambrian and early Ordovician. This paper focuses on the Yeli-Liangjiashan Formation in Area 1. Regionally, the thickness of the Majiagou Formation overlying the Yeli-Liangjiashan Formation is approximately 600 m.

In the Yeli-Liangjiashan Formation in Area 1, the strata have a strike of NW20°, dip direction of 30°, and dip angle of 35°. The exposed strata are distributed in thick layers (the thickness of a single layer reaches 1 m), and the thickness of a single layer in the section is uniform overall. The lithology is mainly dolomite, and the lithology is uniform both vertically and laterally (Figure 4a,b,i). Vertically, the reservoir space exhibits apparent zonation, which can be roughly divided into an upper fractured vuggy zone (Zone 1) and a lower cavity zone (Zone 2). High-angle cracks are developed in the upper fractured vuggy zone, with a maximum length of up to 2 m and a density of up to 5 bars/m. The cracks are curved, and dissolution expansion holes and other holes are often present along the edges of the cracks. Most of the holes are connected to the cracks (Figure 4c). Stratified dissolution pores developed in the cavity zone and were interconnected. The diameters of the pores range from 5 to 15 cm. The dissolution pores are filled with different degrees of multistage secondary calcite, and the boundaries between secondary calcite at different periods are clearly distinguishable (Figure 4d,e). Karst breccias are present in Zone 1 and Zone 2, and the karst breccias are angular to subangular in shape, with the largest diameter reaching 20 cm and the most minor diameter reaching 1 cm. Calcite veins filled and developed along rock fractures and interlayer fractures, and a large number of clay impurities filled the karst breccias (Figure 4f). Elliptic chert nodules are present in the dolomites of the Yeli-Liangjiashan Formation. The nodules are approximately 18 cm in size and are distributed along bedding planes (Figure 4g). The outcrop of the Fengshan Formation in Area 1 (Figure 4h) shows the development of bamboo leaf-shaped dolomites, some of which show disorderly accumulation, some of which show bedding distribution characteristics, and fractures and dissolution cavities are less common than those in the Yeli-Liangjiashan Formation.
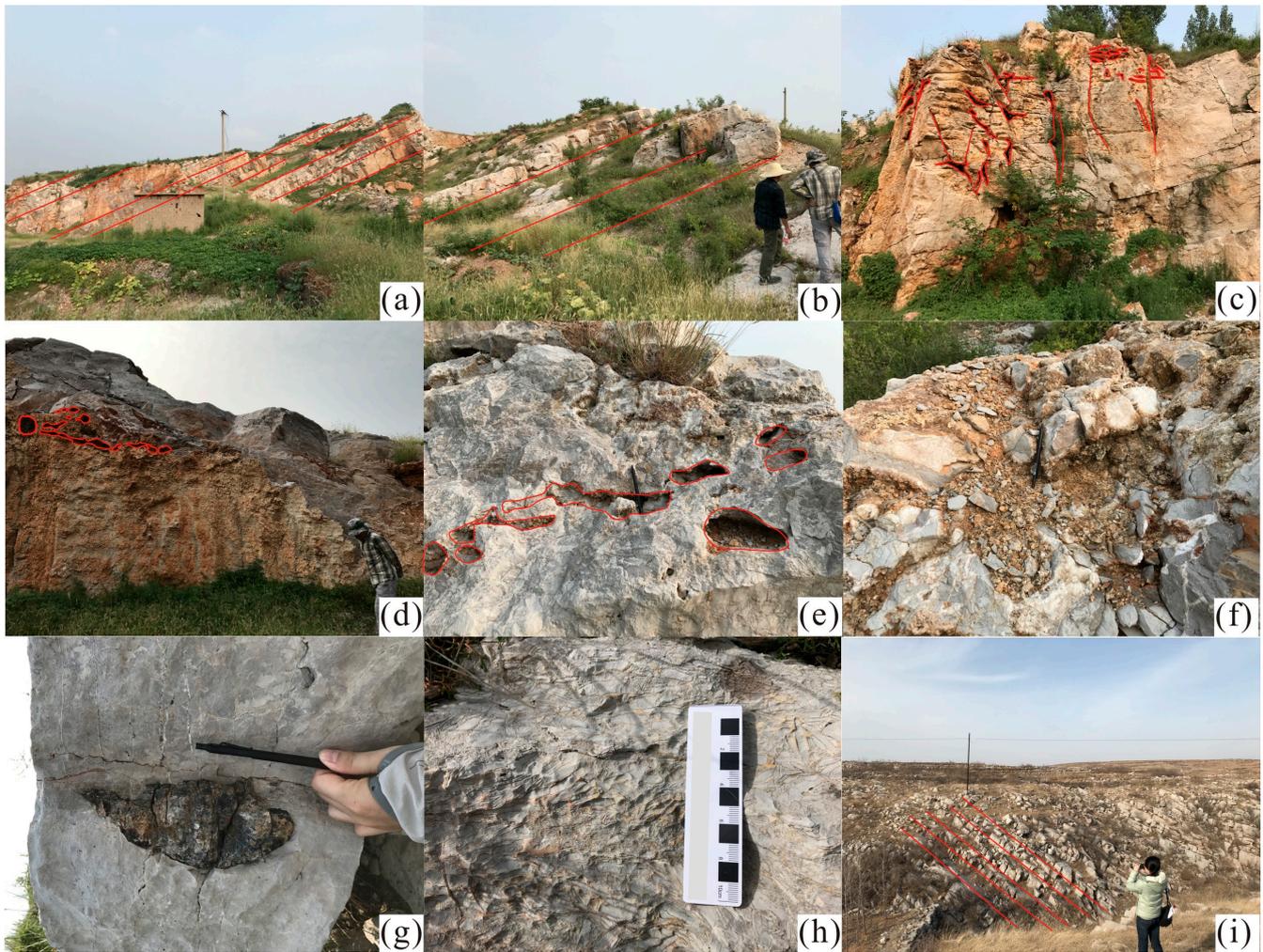
Figure 4. Geological characteristics of the Yeli-Liangjiashan Formation and Fengshan Formation in Matouya area, Xinwen City and Yangzhuang area, Yishui County, Linyi City, Shandong Province. (**a**) The dolomites of Yeli-Liangjiashan Formation are distributed in thick layers; (**b**) Development of dissolved pores and cavities, thick layer distribution of dolomite in Yeli-Liangjiashan Formation; (**c**) Vertical cracks and holes are developed in Liangjiashan Formation; (**d**) The profile of Liangjiashan Formation shows the development of layered dissolved pores; (**e**) Stratified dissolved pores are developed and connected in the Yeli-Liangjiashan Formation; (**f**) Development of karst breccia in Yeli-Liangjiashan Formation; (**g**) Chert nodules are developed in dolomite of Liangjiashan Formation; (**h**) Bamboo leaf-shaped dolomite is developed in Fengshan Formation. (**i**) The dolomites of Liangjiashan Formation are distributed in thick layers. Except for photo (**i**) of Yangzhuang area, other photos are of Matouya area.

4.2. Core Characteristics

(1) Rock types and developmental characteristics

The lithology of the Yeli-Liangjiashan Formation and Fengshan Formation is mainly dolomite, and the most common rock type is crystalline dolomite, followed by granular dolomite and dolomitic breccia with different thicknesses. Among them, the crystalline dolomite is usually gray–gray-white, sugar-like, primarily fine and mesocrystalline, and massive in structure, with dissolution cavity development and sometimes visible cracks filled with calcite or dolomite veins (Figure 5a). Under the microscope, the dolomite is mostly microcrystalline to mesocrystalline (mainly fine to mesocrystalline dolomite), and it is mainly composed of hemiidiomorphic to idiomorphic crystals (Figure 6a–c,e,g,h,l). The crystal type is uniform, and the boundaries between particles are clear, showing point

and line contacts. Granular dolomite with a circular appearance can be observed in the core, and it is mainly gray in color, intergranular and with calcite cement (Figure 5e). The original granular outline of granular dolomite is visible under the microscope; the pores between particles are relatively developed, and no cemented filling is observed (Figure 6k).

Dolomitic breccia mainly developed at the tops of the Yeli-Liangjiashan Formation and Fengshan Formation. According to their genetic types and development locations, two subtypes can be further delineated: karst breccia related to percolation (type 1 karst breccia) and karst breccia related to underflow action (type 2 karst breccia). The characteristics of the two types of karst breccia are significantly different.

Figure 5. Core characteristics of Yeli-Liangjiashan Formation in Chengdao-Zhuanghai buried hill. (**a**) Well CBG100, 2562 m, granular (fine crystalline) dolomite, the high angle crack is connected with the dissolved pore; (**b**) Well CBG5, 2586 m, dolomitic breccia, dissolved pores developed, partially filled with calcite; (**c**) Well CBG5, 2602 m, the dolomitic breccia with good roundness is arranged in a directional manner; (**d**) Well CBG5, 2585.4 m, dolomitic breccia, high degree of calcite vein filling; (**e**) Well CB302, 4002.16 m, intergranular dolomite filled with calcite; (**f**) Well CBG5, 2584.6 m, granular dolomite, subrounded breccia, layered dissolved pores are developed; (**g**) Well CB403, 2759.5 m, the dolomitic karst breccia is interspersed with percolating sand; (**h**) Well CB302, 4001.26 m, limy karst breccia with dissolved pores developed and a small part filled with soil; (**i**) Well CB302, 4001.86 m, limy karst breccia with unfilled pore development; (**j**) Well CBG5, 2601.5 m, limy dolomite cracks are developed, and the cracks are filled with mud; (**k**) Well CBG100, 2560.47 m, dolomite limestone, high angle crack development; (**l**) Well CB244, 2921.27 m, granular (fine crystalline) dolomite, network cracks filled with calcite veins.
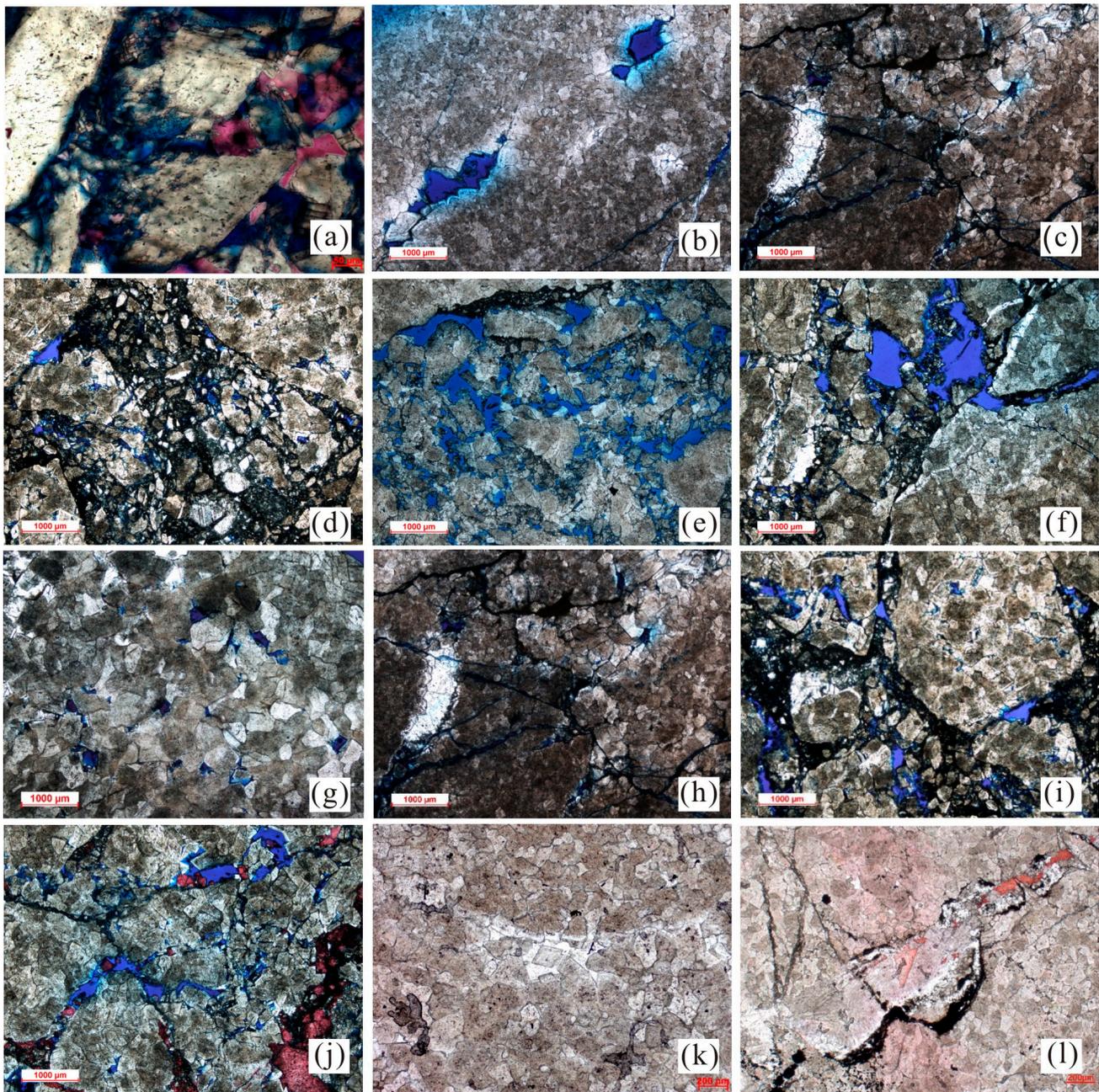
Figure 6. Observation features of Yeli-Liangjiashan Formation in Chengdao-Zhuanghai buried hill under microscope. (**a**) Well CB302, 4001.26 m, dolomitic breccia, calcite is filled in the primary pores of dolomite grains (-); (**b**) Well CB244, 2904.67 m, mesocrystalline dolomite and intercrystalline pore and crack (-); (**c**) Well CB244, 2914.37 m, mesocrystalline dolomite and cracks are developed (-); (**d**) Well CB302, 4008.26 m, the dolomitic karst breccia is filled with protolith debris and the dissolved pore develops (-); (**e**) Well CB302, 4005.35 m, dolomitic karst breccia, intergranular pores are developed, and the breccia is filled with percolating sand (-); (**f**) Well CB302, 4008.26 m, dissolved pores in granular dolomite (-); (**g**) Well CB244, 2925 m, the primary pore in mesocrystalline dolomite is not filled (-); (**h**) Well CB244, 2910 m, the dissolved pore and crack development of mesocrystalline dolomite (-); (**i**) Well CB302, 4008.26 m, dolomitic karst breccia, residual granular dolomite, dissolved pore development (-); (**j**) Well CB302, 4006.5 m, dolomitic karst breccia, intergranular and intragranular pores are filled with calcite (-); (**k**) Well CB244, 2920.6 m, granular dolomite, the particles are relatively complete, the pores developed in the early stage and were partially filled by cement in the later stage (-); (**l**) Well ZG28, 4122.92 m, granular dolomite, the crack is filled with asphalt (-).

Type 1 karst breccia mainly developed in atmospheric freshwater vadose zones. The composition of the breccia is dolomitic or lime-rich, and the breccia has a relatively loose structure, angular shape, and different clast sizes, often showing the characteristics of chaotic and mixed accumulation. The breccia is often filled with mud, sand from percolation, etc., and the dissolution cavities are developed both in the karst breccia and in the interstitials between the clasts in breccia. This breccia type is composed of crystalline dolomite, granular dolomite, granular limestone, and lime dolomite. This type of breccia is found in well CB302 (4001.26–4009.06 m) and well CBG403 (2759.5 m) (Figure 6g–i). In well CB302, this breccia type developed at a depth of nearly 480 m from the paleokarst unconformity interface (3520 m) between the overlying lower Paleozoic and Mesozoic strata. Most clasts are approximately 0.5 cm in diameter, and the clasts are disorderly and unoriented. The breccia has obvious silicification, which is limited to the breccia, or it is filled with mud, dolomite debris, quartz, etc., and no silicification is found. Sometimes, late calcite veins cut through the breccia, dissolution holes are present between the clasts, cracks are present, and oil immersion tests were conducted. The oil immersion test results show that the interval contains oil. Under the microscope, some of the dissolved pores in this type of breccia are filled with calcite, the calcite crystal form is good, some of them are dissolved in the later stage, the boundaries between the breccia particles are clear, and the breccia is filled with argillaceous intercalations, sand from percolation and calcite (Figure 6d,f,i,j).

Type 2 karst breccia is mainly found in the underflow zone. This breccia type is dolomitic or lime-rich, and the clasts are subangular to subrounded. The breccia usually shows an excellent directional arrangement or vertical grain order and generally shows characteristics indicating transport and river redeposition. Well CBG5 contains this type of karst breccia at 2602 m, and CB244 contains this type at 2923.7 m. In these wells, subrounded dolomitic breccia can be observed in a stratified arrangement (Figure 5c,f). Intermediate-like solution pores are present in the breccia, and their sizes are uneven. The breccia is filled with dolomitic debris, etc. Under the microscope, the development of solution pores and microcracks between clasts can be observed. Most of them are effective storage spaces, and some of the particles are filled with calcite (Figure 6b,c,h,k). In the whole core section, there is a noticeable change in the grain size in the longitudinal direction, this change in the grain size has multiple rhythmic characteristics (Figure 5f), and oil immersion tests were conducted on this core section.

(2) Crack types and developmental characteristics

In the core, there are two kinds of cracks with different occurrences in the Yeli-Liangjiashan and Fengshan Formations. The first crack type (crack 1) is usually a curved and high-angle fracture. Soil filling is evident from 2560 to 2562 m in the CBG100 well, and calcite filling occurs. Dissolved pores are often present in the upper and lower parts of such cracks, and the dissolved pores are often connected to the cracks in a bead-like shape. The pores are often filled with clay or saturated sand (Figure 5a,k,j). Under the microscope, these cracks appear to be dissolved and expanded; some of the cracks are filled with mud, dolomite debris, and saturated sand (Figure 6d,f,i,j); and some of the cracks present adequate storage space. The second type of crack (crack 2) is present at 2921.27 m in well CB244 and at 2601.5 m in well CBG5. These cracks usually present medium- and low-angle characteristics, and the edges are relatively straight, showing the feature of cutting each other in a network. The interior is often filled with sparite, dolomite, and other veins. Some calcite grains with good crystal shapes are visible (Figure 5e,l); dissolved pores often develop on both sides of the cracks, and some of them are filled with calcite. These cracks are readily apparent under the microscope in a semifilled-filled state, and some microcracks are filled with bitumen or calcite (Figure 6c,h,l).

(3) Types and developmental characteristics of dissolved pores (holes)

In the core, the solution pores in the Yeli-Liangjiashan Formation and Fengshan Formation can be divided into three categories according to their occurrence. The sizes of the first type of dissolved pore (pore 1) are relatively large. The CBG100 well (2562 m),

CBG5 well (2601.5 m), and ZH101 well (145.75 m) are well developed in many places and have 2–15 mm diameters. The pores are filled with clay or saturated sand, often associated with the first crack type or located below it. The connectivity with the first type of crack (crack 1) is more frequent (Figure 5a,k,j). The second type of dissolved pore (pore 2), with diameters of 1–3 mm, can be observed at 2584.6 m, 2602 m, and other locations in the CBG5 well. The prominent feature of pore 2 is that the dissolved pores are distributed in layers and connected, and their diameters can reach 8–15 mm. The dissolved pores are filled and semifilled, and they are often filled with saturated sand. This type is often found in aligned subangular–subrounded breccias (Figure 5e). The third type of dissolved pore (pore 3), which is present at 4145.75 m in the ZH101 well and at 2586 m in the CBG5 well, varies in size, with the largest being 5 mm and the smallest being 1 mm. This type is filled with a large amount of calcite; some are unfilled, and many contain oil (Figure 5i).

As observed under the microscope, there are many dissolved pores and cracks in the dolomites of the Yeli-Liangjiashan and Fengshan Formations. The edges of the dolomite crystals are irregular and harbor shapes; the cracks are dissolved and expanded, and large dissolution pores are formed along the dissolution–expansion cracks (Figure 6f). The phenomenon of cracks or dissolved pores filled with asphalt can be observed in some sections (Figure 6l). The reservoir space consists of various dissolved pores, dissolution expansion cracks, and intergranular pores of residual granular dolomite, among which the dissolved pores include secondary pores, such as integrated–dissolved pores, mold pores, intergranular dissolved pores, and intragranular dissolved pores. The intragranular dissolved pores are mainly present in the karst breccia dolomites (Figure 6b), and the pore sizes are relatively small, generally between 0.05 and 0.1 mm. Intergranular dissolution pores are mainly present between the granular dolomite and breccia within the residual granular dolomite and dolomitic karst breccias (Figure 6c,d,i), showing varying sizes and uneven distributions under the microscope. The pore sizes are generally 0.2–0.8 mm, with a maximum of 2 mm, and some of the pores are filled or half-filled by calcite idiomorphic crystals (Figure 6d). The mold pores are mainly present in the dolomitic karst breccias, and relatively small clasts are entirely dissolved, leaving only their appearance in the remaining breccia (Figure 6f). Intergranular and intragranular dissolved pores are mainly present in fine-grained and medium-grained dolomites, with relatively small pore sizes. Generally, they are approximately 0.1 mm long, and some of them are filled with gypsum (Figure 6g,h).

At both the core scale and the hand sample scale, there are many types of reservoir spaces in the dolomites of the Yeli-Liangjiashan Formation and Fengshan Formation. They are interconnected and interleaved, forming a composite space-like network in the reservoir, with crack-cavity type (Figure 5a,j), cavity type (Figure 5b,f), and crack type spaces (Figure 5l,k). Among them, the crack-cavity and crack types are present in reservoirs where matrix pores are not present or near faults. The cavity type is relatively prevalent in the dolomite reservoirs of the Yeli-Liangjiashan and Fengshan Formations or inside the faults.

Due to the variety of carbonate reservoir types in the Yeli-Liangjiashan Formation and Fengshan Formation, their reservoirs are highly heterogeneous, and their reservoir parameters, such as porosity and permeability, vary widely. Based on the existing routine core analysis data, 24 samples from three core wells in the Yeli-Liangjiashan Formation and Fengshan Formation in the study area were statistically analyzed. The maximum porosity was 12.2%, the minimum was 1.1%, the maximum permeability was $266.659 \times 10^{-3} \ \mu m^2$, and the minimum permeability was $0.025 \times 10^{-3} \ \mu m^2$ (Table 1). The wide variation range in porosity and permeability fully indicates the heterogeneity and complexity of reservoir types in space.
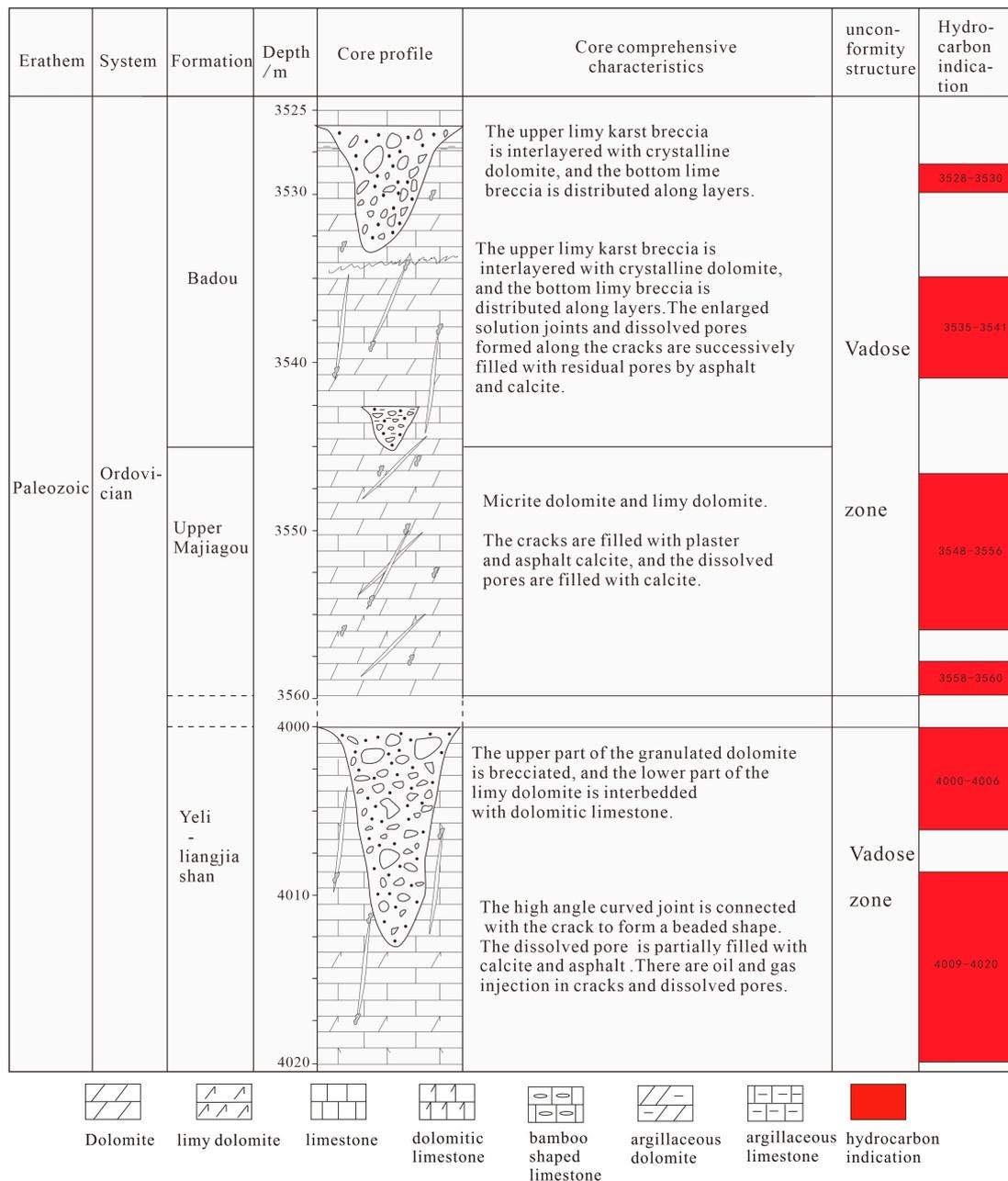
(4)   Longitudinal zoning features

Through observation and analysis of the core characteristics of several wells, according to the characteristics of karst breccia development, the reservoir in the study area has the characteristics of karst zonation in the vertical direction, that is, the upper vadose zone and the lower underflow zone. Statistics show that the vadose zone and underflow zone

can be present independently, either simultaneously or separately in the Yeli-Liangjiashan Formation or Fengshan Formation, (Figures 7 and 8).

Table 1. Statistical table of porosity and permeability of some wells in the Yeli-Liangjiashan Formation.

Well	Formation	Porosity (%)				Permeability/$\times 10^{-3}$ μm^2			
		Minimum Value	Maximum Value	Sample Quantity	Mean Value	Minimum Value	Maximum Value	Sample Quantity	Mean Value
CB244	Yeli-Liangjiashan Formation	1.1	12.2	18	4.32	0.075	266.659	16	21.535
CB39	Yeli-Liangjiashan Formation	2.3	4.6	4	3.15	0.025	8.01	4	2.043
CBG6	Yeli-Liangjiashan Formation	9.4	2.5	4	4.48	1.545	1.545	1	1.545

Figure 7. Well CB302 core–karst composite column diagram.

Erathem	System	Formation	Depth /m	Core profile	Core comprehensive characteristics	unconformity structure	Hydrocarbon indication
Paleozoic	Ordovician	Yeli-liangjiashan	2900–2927		Granular dolomite(fine grain)，Oil-immersion, Along the crack development and expansion of the dissolved pore is filled with calcite.	underflow zone	2900–2902
					Granular dolomite(fine grain)，layered dissolved pore development, cracks are filled with calcite and organic matter.		
					Granular dolomite(fine grain)，the pores and cracks are relatively developed, and in a half-filled state, oil immersion.		2903–2921
					There are more pores and cracks in granular dolomite(fine grain)，calcite veins are developed, and there is oil infiltration in pores and cracks.		
					Granular dolomite(fine grain)，Occasionally, a dissolved pore with a diameter of about 5mm was found；Locally, microcracks can be seen in a semi-filled state，some cracks have oil infiltration.		
					Granular dolomite(fine grain)，pores do not develop, and micro-cracks develop.		
					Dolomitic karst breccia are developed, filled with dolomitic clastics between breccias. There are dolomitic breccia in the bedding dislocated by cracks.		
					Interbedded granular dolomite and granular dolomite, dolomitic karst breccia, has the characteristics of unidirectional flow along the bedding distribution.		

Legend: Dolomite; limy dolomite; limestone; dolomitic limestone; bamboo shaped limestone; argillaceous dolomite; argillaceous limestone; hydrocarbon indication
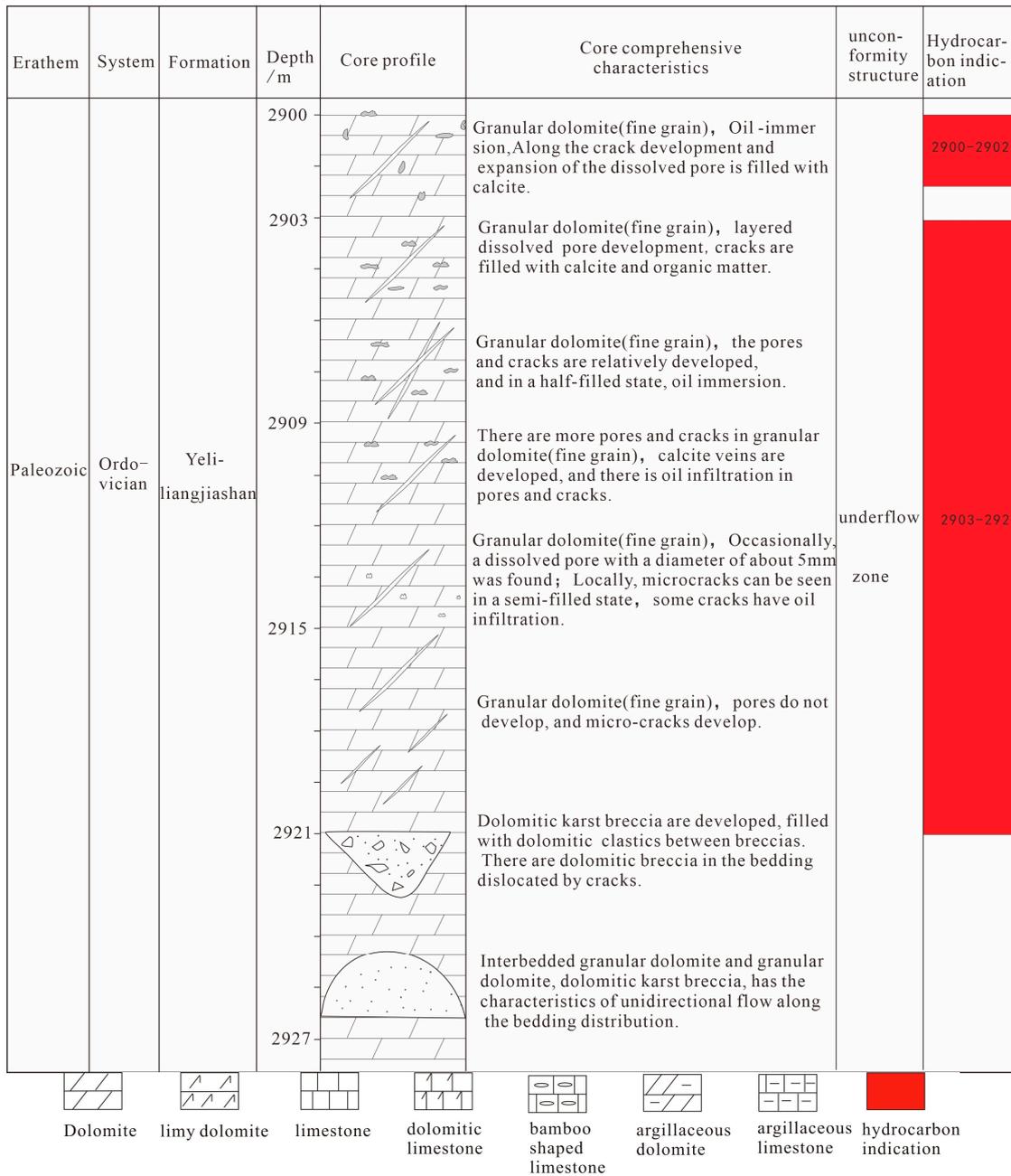
Figure 8. Well CB244 core–karst composite column diagram.

Type 1 karst breccia is present in the vadose zone, and the longitudinal reservoir development characteristics of the Yeli-Liangjiashan Formation in the CB302 well are the most significant (Figure 7). Type 1 dolomitic karst breccia, limy dolomite and dolomitic limestone are present in the well, and type 1 breccia is present in the 4001.26–4009.06 m segment. In this zone, high-angle curved cracks (crack 1) are mainly present, and dissolved pores (pore 1) are present in the upper or lower parts of the cracks in the longitudinal direction of their development. They are connected with cracks (crack 1). The most significant pores reach 15 mm in diameter, and the pores are filled with mud or calcite, but there are still residual pores (pore 3) and oil that is present. In addition to high-angle curved cracks (crack 1), low-angle network cracks (crack 2) are also present but are not unique. According to the drilling data, leakage of 113 m^3 occurred when this zone of the karst breccia section was drilled.

Karst breccia type 2 and layered dissolved pores are present in the underflow zone. This zone is revealed by the longitudinal reservoir development characteristics of well CB244 (Figure 8). The lithologies are mainly granular (fine-grained) dolomite and granular (sand-dust) dolomite, with network cracks (crack 2) and layered dissolved pores (pore 2). Cracks (crack 2) and dissolved pores (pore 2 and pore 3) are half-filled with asphalt and calcite filling materials. In the 2921.37–2923.67 m segment, dolomitic karst breccia is present in a subangular shape, with pore 3 in the breccia, and the pores are filled with calcite. In the 2923.67–2925.27 m section, the granular (sand debris) dolomite and micritic dolomite are interstratified, and the dolomitic karst breccia is forward-distributed. The clasts are subangular, with excellent roundness, and they show the characteristics of unidirectional water flow. The breccia is filled with sparry calcite cement.

4.3. Isotopic Geochemical Characteristics

According to the geochemical characteristics of C and O isotopes in rock samples from the Yeli-Liangjiashan Formation and Fengshan Formation (Table 2), the isotopic variations in C and O in the Yeli-Liangjiashan Formation are greater, with $\delta^{13}C$ values varying from −9.92‰ to −0.14‰ and $\delta^{18}O$ values varying from −15.46‰ to −7.97‰. The $\delta^{13}C$ and $\delta^{18}O$ values range from −0.56‰ to 1.34‰ and from −14.23‰ to −6.24‰, respectively, in the Fengshan Formation. According to the Sr isotope geochemical characteristics of the Liangjiashan Formation and Fengshan Formation samples (Table 3), the $^{87}Sr/^{86}Sr$ values of the Yeli-Liangjiashan Formation have extensive variation, with values ranging from 0.7103 to 0.7145. The $^{87}Sr/^{86}Sr$ values of the Fengshan Formation vary between 0.7103 and 0.7144.

Table 2. Geochemical characteristics of C and O isotopes of Yeli-Liangjiashan Formation and Fengshan Formation.

Serial Number	Sample Number	Lithology	Stratum	Sampling Depth (m)	$\delta^{13}C_{v\text{-PDB}}$ (‰)	$\delta^{18}O_{v\text{-PDB}}$ (‰)	Remark
1	HB19-1	dolomite	Yeli-Liangjiashan Formation	-	−9.92	−8.84	
2	HB19	dolomite	Yeli-Liangjiashan Formation	-	−7.68	−7.97	According to Zhang, Y.F., and Wang, Q.C., 2007 [38]
3	HB12	dolomite	Yeli-Liangjiashan Formation	-	−5.24	−9.97	
4	HB09-1	dolomite	Yeli-Liangjiashan Formation	-	−7.89	−8.92	
5	HB09	dolomite	Yeli-Liangjiashan Formation	-	−7.45	−9.51	
6	CB302-10	dolomite	Yeli-Liangjiashan Formation	4003.3	−1.29	−13.18	
7	CB302-4	dolomite	Yeli-Liangjiashan Formation	4006.5	−1.28	−12.39	
8	CB302-8	dolomite	Yeli-Liangjiashan Formation	4005.4	−0.14	−9.78	
9	CB302-1	dolomite	Yeli-Liangjiashan Formation	4008.3	−0.46	−9.56	
10	CB302-21	dolomitic breccia	Yeli-Liangjiashan Formation	4002	−0.96	−10.42	This study
11	CB302-15	dolomite	Yeli-Liangjiashan Formation	4003.34	−2.43	−13.24	
12	ZH101-2	dolomite	Yeli-Liangjiashan Formation	4076.21	−2.3	−15.46	
13	ZH101-3	dolomitic breccia	Yeli-Liangjiashan Formation	4076.91	−2.59	−14.87	
14	CBG100-1	dolomite	Fengshan Formation	2561.68	−0.02	−7.31	

Table 2. *Cont.*

Serial Number	Sample Number	Lithology	Stratum	Sampling Depth (m)	$\delta^{13}C_{v\text{-}PDB}$ (‰)	$\delta^{18}O_{v\text{-}PDB}$ (‰)	Remark
15	CBG100-2	dolomite	Fengshan Formation	2561.68	−0.01	−6.59	
16	CBG100-3	dolomite	Fengshan Formation	2561.68	−0.38	−6.73	
17	CBG100-4	dolomite	Fengshan Formation	2561.68	−0.05	−6.24	
18	CBG100-5	dolomite	Fengshan Formation	2566.27	−0.32	−6.88	
19	CBG100-6	dolomite	Fengshan Formation	2566.17	−0.22	−8.1	
20	CBG100-7	dolomite	Fengshan Formation	2566.17	−0.53	−6.59	
21	CBG100-8	dolomite	Fengshan Formation	2566.17	−0.56	−7.41	This study
22	ZG39-1	limestone	Fengshan Formation	4338.2	0.27	−10.07	
23	ZG39-2	limestone	Fengshan Formation	4341.1	0.21	−10.6	
24	ZG39-3	limestone	Fengshan Formation	4343.3	0.44	−10.19	
25	ZG39-4	dolomitic limestone	Fengshan Formation	4345.9	0.7	−14.23	
26	ZG39-5	limestone	Fengshan Formation	4349.3	1.17	−12.57	
27	ZG39-6	limestone	Fengshan Formation	4351.8	1.34	−10.9	

Table 3. Sr isotope geochemical characteristics of Yeli-Liangjiashan Formation and Fengshan Formation.

Serial Number	Sample Number	Lithology	Stratum	Sampling Depth (m)	$^{87}Sr/^{86}Sr$
1	CB302-1A	dolomite	Yeli-Liangjiashan Formation	4001.2	0.7103
2	CB302-2A	dolomite	Yeli-Liangjiashan Formation	4001.46	0.7133
3	CB302-3A	dolomite	Yeli-Liangjiashan Formation	4004.45	0.7145
4	CB302-4A	dolomite	Yeli-Liangjiashan Formation	4008.5	0.7138
5	CB302-5A	dolomite	Yeli-Liangjiashan Formation	4001.5	0.7105
6	SHG 2-1A	dolomite	Yeli-Liangjiashan Formation	2404	0.7097
7	SHG2-2A	dolomite	Yeli-Liangjiashan Formation	2407.9	0.7093
8	SHG2-3A	dolomite	Yeli-Liangjiashan Formation	2408	0.7116
9	ZG39-1	dolomite	Fengshan Formation	4338.2	0.7108
10	ZG39-2	dolomite	Fengshan Formation	4341.1	0.7107
11	ZG39-3	dolomite	Fengshan Formation	4343.3	0.7106
12	ZG39-4	dolomitic limestone	Fengshan Formation	4345.9	0.7144
13	ZG39-5	dolomite	Fengshan Formation	4349.3	0.7103
14	ZG39-6	dolomite	Fengshan Formation	4351.8	0.7116
15	ZH10	dolomite	Fengshan Formation	4658.14	0.7113
16	ZG39-7	dolomite	Fengshan Formation	4359.2	0.7108
17	ZG39-8	dolomite	Fengshan Formation	4361.8	0.7117
18	ZG39-9	dolomite	Fengshan Formation	4358.1	0.7126

5. Discussion

5.1. Evidence of the Record of Huaiyuan Movement

(1)   Geological evidence of the Huaiyuan Movement

Regionally, different parts of the Yeli-Liangjiashan Formation and Lower Majiagou Formation overlie different strata on the North China Platform, resulting in regional parallel unconformities between the Yeli-Liangjiashan Formation and Fengshan Formation, and the same is true between the Lower Majiagou Formation and Yeli-Liangjiashan Formation. For example, Osleger (1991) [39] noted that at the end of the Cambrian period, a global sea level decline occurred at the bottom interface of the Ordovician strata. Liu et al. (1997) [40]

proposed a paleokarst-related unconformity at the top of the Ordovician Liangjiashan Formation in the North China Platform. The unconformity is parallel, and there is an apparent change in lithology at the boundary. Underly the boundary are medium-fine crystalline dolomites with chert bands, which have different degrees of karstification. According to Mei and Ma (2003) [41], on the basis of the contact relationship between the Cambrian and overlying strata in different regions of the North China Platform, from the Xishan section in Beijing to the Zhang Xia section in Tai'an Shandong, the Jiawang section in Xuzhou, and the Huainandongshan section (see profile 1 in Figure 1 for the specific location), there was a short period of exposure to different degrees between the Cambrian and the Ordovician, especially in Shandong Province. There was more prolonged exposure between the deposition of the Fengshan Formation and the Yeli-Liangjiashan Formation than between that of the Xuzhou and Zhunnan sections, thus forming an unconformity between them.

Through field observations of the Yeli-Liangjiashan Formation in the Matouya area, Xinwen city, Shandong Province, and Yangzhuang, Yishui County, Linyi city, Shandong Province, many karst breccias are found in the Yeli-Liangjiashan Formation. The vadose zone and underflow zone can be delineated (Figure 4), indicating that after the deposition of the Yeli-Liangjiashan Formation, many karst breccias formed in the Yeli-Liangjiashan Formation. It was briefly uplifted to the surface and weathered and denuded. According to the seismic data in the study area, different parts of the Lower Majiagou Formation overlie the Fengshan Formation and Yeli-Liangjiashan Formation, resulting in regional unconformities between the Lower Majiagou Formation and the Fengshan Formation and Yeli-Liangjiashan Formation. For example, in the CB271-CBG403-CBG4 North–South seismic profile (Figure 9, see profile in Figure 10 for the specific location), the bottom seismic reflection axes of the lower Paleozoic Badou Formation, Upper Majiagou Formation, Lower Majiagou Formation, Yeli-Liangjiashan Formation, and Fengshan Formation are visible. In the northeastern area of the CBG4 bulge, the Cambrian and Ordovician Yeli-Liangjiashan Formation forms wedges from southwest to northeast. The Formation gradually thins in the northeast direction and truncates and is overlapped by the Majiagou Formation. This situation is more common in the lower Paleozoic strata of the Chengdao-Zhuanghai buried hill, indicating that tectonic uplift and exposed denudation occurred during the Huaiyuan Movement [42]. In the Chengdao-Zhuanghai buried hill, there are three overlapping regional unconformity surfaces at the top of the Ordovician System, the bottom of the Majiagou Formation, and the top of the Cambrian System. In the past, people thought that the unconformity in this area formed during the late Caledonian Movement [25]. However, it may be the unconformity of the Huaiyuan Movement (early Caledonian Movement) and the late Caledonian Movement superimposed together.

According to the observations of solid drill cores, karst breccias of different sizes have been found in the Fengshan Formation and Yeli-Liangjiashan Formation. Saturated sand structures between breccias are present, and karst breccias are the most direct manifestation of the strata's exposure to atmospheric freshwater leaching [17]. The existence of many karst breccias in the Yeli-Liangjiashan Formation and Fengshan Formation indicates that the studied strata must have been subjected to atmospheric freshwater leaching for some time after deposition, resulting in the formation being subjected to dissolution. During the longitudinal leaching and dissolution of atmospheric freshwater, the mud and sand on the weathering crust formed by weathering permeated downward into the cracks and filled in the karst breccia.

The vertical zonation of karst indicates the record of the Huaiyuan Movement. Many studies on modern and ancient karst regions have been conducted by different geologists. According to the extent of karst system development and modes of groundwater movement and karst action, geologists have suggested that there are zones of hydrodynamic action in vertical karst activity, and these can be delineated from top to bottom: surface karst zone–vadose karst zone–runoff karst zone–underflow karst zone [43]; surface karst zone–vertical percolation zone–runoff solution zone–underflow solution zone [44];

or surface karst zone–vertical percolation zone–horizontal underflow zone–deep slow flow zone [21]. The drill core shows that similar zones of karst hydrodynamic action are visible in wells CB244, CB302, CB307, and ZH102 in the study area. The vertical vadose zone and horizontal underflow zone can be divided from top to bottom (Figures 7 and 8). The horizontal underflow zone is affected by the mode of horizontal flow. Horizontal layered dissolved pores and underground rivers are present, and subrounded karst breccia is present and displays vertical characteristics of normally graded bedding (Figure 5f). These data show the characteristics of long-distance transport and river deposition. This zonation results from formation uplift and denudation after deposition and the long-term transformation of atmospheric freshwater.
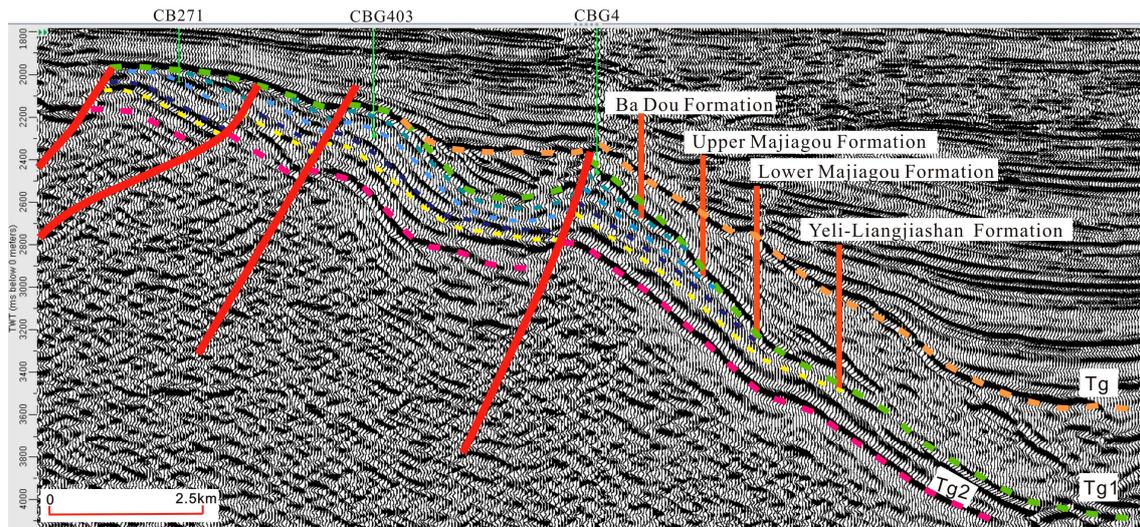
Figure 9. Seismic reflection characteristics of each section in the lower Paleozoic in Chengdao-Zhuanghai buried hill (Tg—Top of the Upper Paleozoic, Tg1—Top of the Lower Paleozoic, Tg2—Top of Mantou Formation).
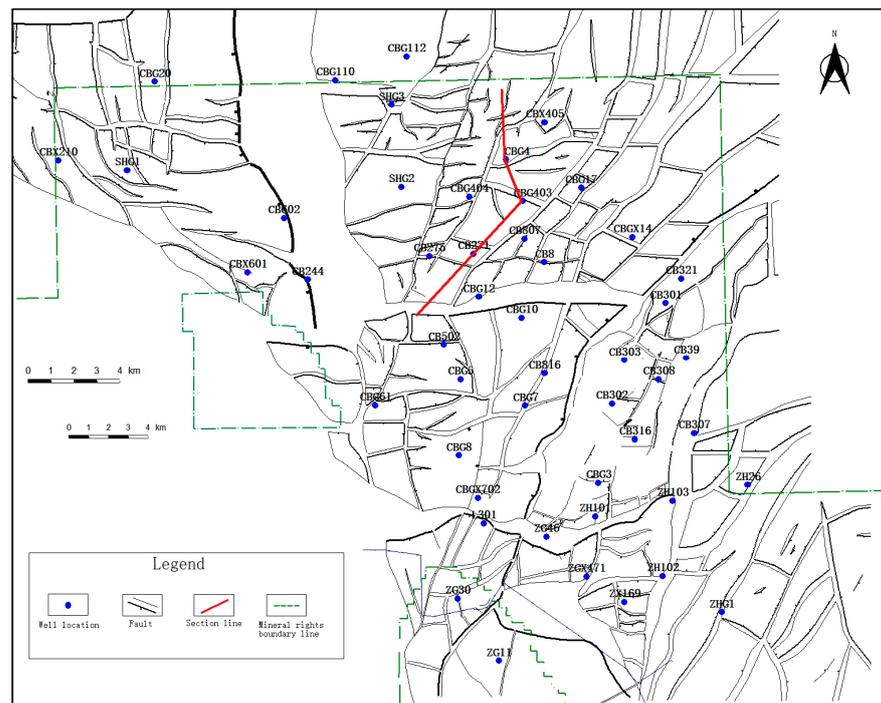
Figure 10. Structure map of top of the Lower Paleozoic of Chengdao-Zhuanghai buried hill.

Observing the outcrop and drill core, the unconformity formed during the Huaiyuan movement exists in the study area, consistent with previous studies. Further compared with previous studies, it can be seen from the seismic and tectonic characteristics of the study area and the zonation of core karstification that there were at least two significant periods of supergene karstification during the Huaiyuan movement, which resulted in unconformity between the Fengshan Formation and Yeli-Liangjiashan Formation, and between the Yeli-Liangjiashan Formation and overlying strata.

(2)   Geochemical evidence of the Huaiyuan Movement

Isotopic analysis of C, O, and Sr in the Yeli-Liangjiashan Formation reveals that $\delta^{13}C$ values range from $-9.92‰$ to $-0.14‰$, $\delta^{18}O$ values range from $-15.46‰$ to $-7.97‰$, and $^{87}Sr/^{86}Sr$ values range from 0.7103 to 0.7145. Studies have shown that in Ordovician seawater, $\delta^{13}C$ values vary from approximately $-3‰$ to $3‰$, $\delta^{18}O$ values vary from approximately $-11‰$ to $-3.6‰$ [45], and the average $^{87}Sr/^{86}Sr$ value is 0.7085 [46]. The $\delta^{13}C$ values of some carbonate rocks in the Yeli-Liangjiashan Formation are lower than those of seawater during the same period, and the abnormally low $\delta^{13}C$ values ($-5.24‰$–$9.92‰$) are mainly related to atmospheric freshwater [47]. The $\delta^{18}O$ values of the Yeli-Liangjiashan Formation are greater than those of seawater from the same period, and the $^{87}Sr/^{86}Sr$ values are more enriched than the $^{87}Sr/^{86}Sr$ values in seawater from the same period (Figure 10), indicating that the Yeli-Liangjiashan Formation has been affected by alteration by atmospheric freshwater, which is more enriched in $^{87}Sr/^{86}Sr$ than seawater [48–50]. The diagram showing the Sr–O isotope relationship (Figure 11) reveals that some samples have Sr–O isotope characteristics that are similar to those of unmodified marine carbonate rocks; others have abnormally high and abnormally low values, which may be equivalent to the Sr–O isotope characteristics of atmospheric freshwater, and some samples display values between the two. These results show that this part of the sample is an intermediate product of the water–rock reaction.
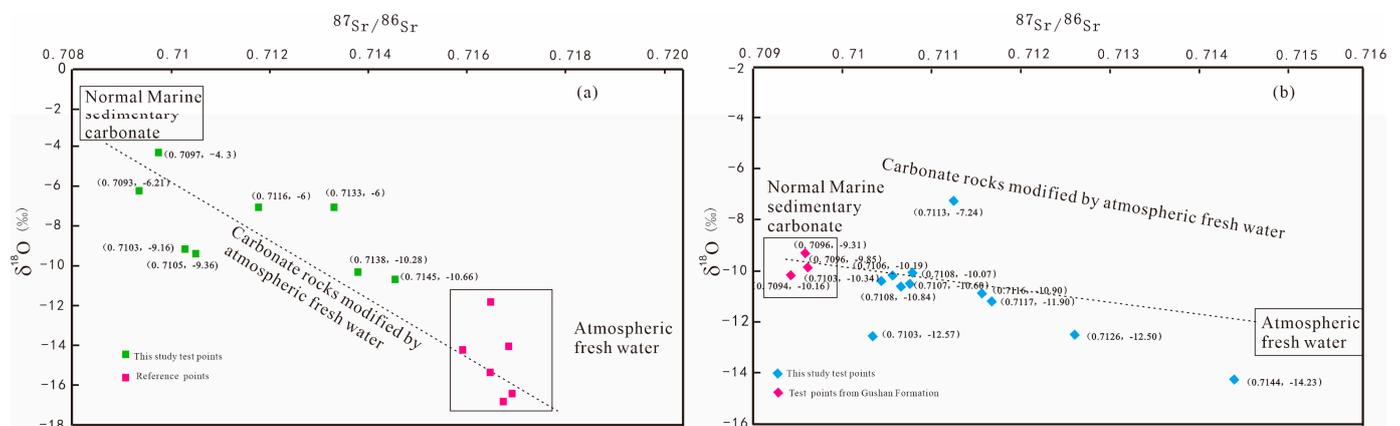

Figure 11. Sr−O isotope correlation between Yeli-Liangjiashan Formation (**a**) and Fengshan Formation (**b**).

The results show that the $\delta^{13}C$ values range from $-0.56‰$ to $1.34‰$, the $\delta^{18}O$ values range from $-14.23‰$ to $-6.24‰$, and the $^{87}Sr/^{86}Sr$ values range from 0.7103–0.7144. The literature shows that the $^{87}Sr/^{86}Sr$ values of Cambrian seawater are between 0.7081 and 0.7093 [45,46], the $\delta^{13}C$ values vary from $-2‰$ to $0‰$ (Veizer et al., 1999) [45], and the mean $\delta^{18}O$ value is $-9.8‰$. The $\delta^{18}O$ value of the Fengshan Formation carbonate rocks is more negative than that of seawater from the same period, and the $^{87}Sr/^{86}Sr$ values are more enriched than the $^{87}Sr/^{86}Sr$ values of seawater from the same period, indicating that the Fengshan Formation was also undergoing alteration by atmospheric freshwater [49–51]. The Sr–O isotopic correlation diagram (Figure 11) shows that the Sr–O isotopic relationship characteristics are similar to those of the Yeli-Liangjiashan Formation, and some samples show that the values are the product of water–rock transformation.

According to the geochemical characteristics of C, O, and Sr isotopes mentioned above, the carbonates of both the Yeli-Liangjiashan Formation and the Fengshan Formation have been reformed by atmospheric freshwater. The difference in the $^{87}Sr/^{86}Sr$ values between the atmospheric freshwater of the Yeli-Liangjiashan Formation and the Fengshan Formation is reflected by the covariant Sr–O isotope relationship, which indicates that they were modified by atmospheric freshwater in the same period.

When we determined the range of isotopic values of the supergene karstification influenced by the Huaiyuan movement, which is characterized as "carbon–oxygen isotope poor, strontium isotope rich", we can preliminarily speculate that the carbonate rocks with such geochemical characteristics are suitable reservoirs in the Yeli Liangjiashan Formation and Fengshan Formation. Studying the distribution law of high-quality reservoirs in the future is beneficial.

(3) Evidence of the forming time

In earlier studies on the supergene karstification of the lower Paleozoic strata in the Jiyang Depression, many geologists noted the existence of breccia at the top of the Yeli-Liangjiashan Formation and Fengshan Formation, and some of them have classified it as a breccia of tectonic origin. Although most of them define it as karst breccia, it is believed that the formation process was closely related to supergene karstification in the Indosinian and Himalayan periods. Many studies have shown that the depth of influence of supergene karstification caused by atmospheric freshwater on strata is approximately 150 m [42,48]. In well CB302 in the study area, a set of gray and gray karst breccia that is approximately 109 m thick developed continuously in the Yeli-Liangjiashan Formation and Fengshan Formation (Figure 7), of which the karst breccia in the Fengshan Formation is approximately 90 m thick. The set of karst breccia lies 488 m below the unconformity between the Mesozoic and lower Paleozoic strata (late Caledonian–early Hercynian and Indosinian). In addition, the Majiagou Formation overlying this set of karst breccia contains mostly gypsum salt and gypsum dolomite layers acting as water barriers. Due to the depth of karst processes at the top of the Majiagou Formation and the existence of multiple layers acting as water barriers in the Majiagou Formation, the karst processes occurring at the top of the Majiagou Formation cannot affect the Yeri-Liangjiashan Formation and Fengshan Formation. Therefore, the large sets of karst breccia in the Yeli-Liangjiashan Formation and Fengshan Formation likely formed during the Huaiyuan Movement, and they were likely the products of supergenetic activity in the late Yeli-Liangjiashan Formation or the late Fengshan Formation.

In the lower Paleozoic strata of the Jiyang Depression, the C and O isotopes of carbonates modified by atmospheric freshwater in the Hercynian and Xishan Stages show a positive correlation, and their C and O isotope covariant relationships (the detailed characteristics of which will be discussed separately) are obviously different from the C and O isotope covariant relationships formed by paleokarstification in the long Huaiyuan period. In the diagram of the C-O isotope covariant relationship between the Yeli-Liangjiashan Formation and Fengshang Formation modified by long-term atmospheric freshwater (Figure 12), two trend lines with different slopes are visible: one trend line with a positive slope and the other trend line with a negative slope (Figure 12). These results indicate that the Yeli-Liangjiashan Formation and Fengshan Formation were subjected to the effects of modification and superposition by at least two atmospheric freshwater fluids with different C and O isotopes. Among them, at the sample point in well CB302 (Table 2), the strata overlying the Ordovician strata are Mesozoic strata, the depth of the boundary is 3520 m, and the sampling points are in the Yeli-Liangjiashan Formation (approximately 4003 m), according to which the lower Paleozoic–Mesozoic unconformity is approximately 500 m deep. According to previous studies, the depth of influence of atmospheric freshwater leaching is approximately 150 m. The test results show that the sample point in well CB302 plots on the trend line of atmospheric freshwater, with a negative slope (Figure 12). It can be concluded that the time of atmospheric freshwater occurrence in this period was the Huaiyuan Movement, that is, the early Caledonian Movement. The values of C and O

isotopes in this sample were not affected by late supergenetic karstification. On this trend line, C and O isotopes constitute a good negative linear correlation. One end represents the initial rock sample, while the other end represents the long-term atmospheric freshwater end. The C and O isotopes of the initial rock sample are approximately −1‰ and −12‰, respectively. The C and O isotopic values are approximately −10‰ and −9‰, respectively, which are obviously different from the C and O isotopic values of the Hercynian and Xishan Stages. Therefore, the carbonate reservoirs of the Yeli-Liangjiashan Formation and Fengshan Formation are the direct products of the uplift and denudation in the Huaiyuan period (early Caledonian Movement) and the transformation of supergene karstification.
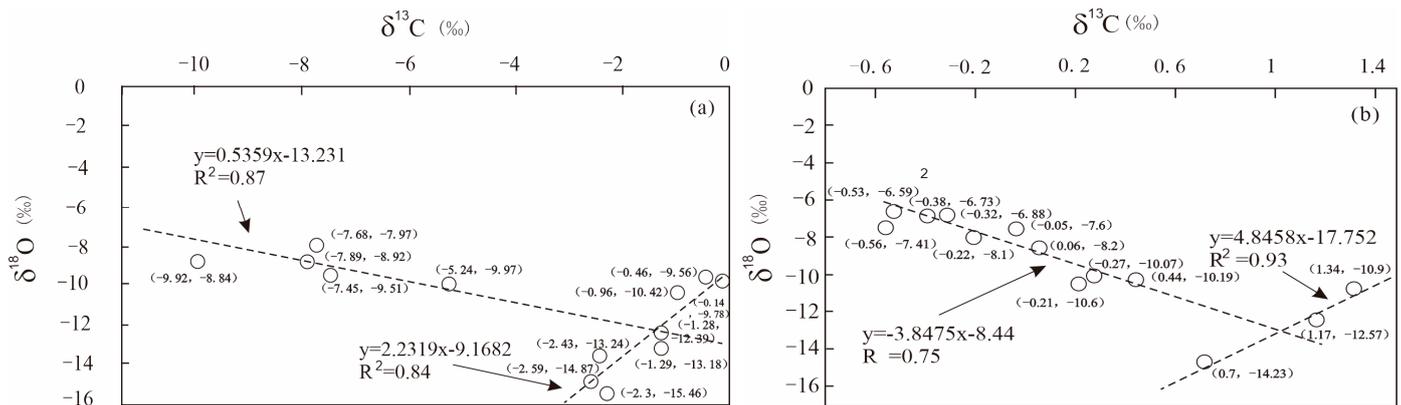
Figure 12. C−O isotope covariant relationship between Yeli−Liangjiashan Formation (**a**) and Fengshan Formation (**b**).

5.2. Influence and Control of Huaiyuan Movement on Reservoir

Through the exploration of peripheral outcrops, core observations, microscopic observations of thin sections, geochemical analysis and analysis of drilling data, the reservoirs of the Yeli-Liangjiashan Formation and Fengshan Formation were determined to be controlled by the original sedimentary facies, dolomitization and supergene karstification.

In the (early Paleozoic) late Cambrian–Early Ordovician sedimentary period, the overall sedimentary environment was an epicontinental sea. In the early sedimentary stages of the Fengshan Formation and Yeli-Liangjiashan Formation, the aquatic environment was relatively stable, the sedimentary facies mainly developed in an open platform environment, and the original lithology was mainly fine-micritic limestone. This study provides a foundation for developing high-quality reservoirs in the study area [52–54]. At the end of the sedimentary period of the Fengshan Formation, the Huaiyuan Movement began and continued until the deposition of the Majiagou Formation. Several seabed uplifting, storm turbulence, and uplift-denudation events affected the entire North China Platform in eastern China [32,33], and diagenesis occurred during this process, including dolomitization and supergene karstification, which actively transformed the reservoir in the studied interval. In general, two critical sedimentary facies changes, dolomitization and supergene karstification, occurred in the late sedimentary period of the Fengshan Formation and the late sedimentary period of the Yeli-Liangjiashan Formation.

In the late sedimentary period of the Fengshan Formation and Yeli-Liangjiashan Formation, tectonic movement caused water turbulence and seabed uplift. Significant changes occurred in the sedimentary facies of the study area: (1) water turbulence and powerful hydrodynamic forces transformed some of the preformed fine-micritic limestones into limestone with a granular structure, and then the deposited sparry granular limestone accumulated to form granular beach facies; (2) the increase in the seabed (sea level decrease) led to the further development of evaporative platform and restricted platform (restricted lagoon) sedimentary facies in the sedimentary environment of the study area based on the open platform facies that formed in the epicontinental sea environment.

When the sea level in the evaporative and restricted platform environments was relatively high, quasi-simultaneous dolomitization due to evaporation occurred, and the fine micrite changed to fine-micritic dolomite and limy dolomite [55,56]. When the sea level was low and the evaporative platform or restricted platform environment was exposed to the surface, the water salinity increased, and the fine micrite that developed in the platform was dolomitized by backflow osmosis to form limy dolomite and fine micritic dolomite [55]. The granular beach facies formed above the wave base in a high-energy aquatic environment, and the granular limestone that developed in this environment was dolomitized under the continuous backflow infiltration of high-energy seawater [26,56–59], as well as the formation of granular dolomite, the development of primary pores between grains, and better reservoir performance [60–64]. According to the thin-section microscopic identification results, in addition to fine crystalline dolomite, mesocrystalline dolomite also occurs in the granular dolomite of the Yeli-Liangjiashan Formation and Fengshan Formation (Figure 6), and its crystals are well formed. Therefore, burial dolomitization occurred in the late study interval [65–67], recrystallization occurred between mud and fine-grained dolomite, and the grains became coarse, forming the mesocrystalline dolomite observed today. After various types of dolomitization occurred in the study interval, the developed lithologies included granular dolomite, medium-fine crystalline dolomite, mud-microcrystalline dolomite, and limy dolomite. Among them, granular dolomite has pores, a good intergranular three-dimensional network pore structure, smooth pore fluid migration, and good original reservoir performance [68]. The reservoir performance of medium-fine crystalline dolomite is second, and the original reservoir conditions of mud (micro)crystalline dolomite are relatively poor [69,70].

The local surface environment emerged and suffered from leaching by atmospheric freshwater, resulting in supergene karstification, which had a positive effect on the transformation of carbonate reservoirs [26,50,51,71], wherein the supergene karstification in the late Yeli-Liangjiashan Formation lasted longer and was more intense than that in the late Fengshan Formation. Apparent karst zones (vadose zone and underflow zone) developed vertically on the tops of the two Formations. Because the dolomitization of the Fengshan Formation was less intense than that of the Yeli-Liangjiashan Formation, the lithology of the dolomite of the Fengshan Formation is lower than that of the Yeli-Liangjiashan Formation. For granular beach facies dolomite, when subjected to supergene karstification, atmospheric freshwater permeated along cracks, intergranular pores formed in the vadose zone, and dissolution occurred, forming cavity-type and crack-cavity-type reservoir space combinations, forming angular karst breccia in the sinkhole and dissolved pores and caves in the areas between sinkholes (Figure 13b). The infiltrated atmospheric freshwater is prone to stratified flow in the underflow zone. Due to the development of the primary pores in the granular dolomite of the granular beach facies, water flows along the existing internal pores, and dissolution occurs, forming a stratified dissolved pore zone or karst cave zone, which results in leakage during exploration and drilling in the oilfield. In the underflow zone, high-quality porous reservoirs easily form. Therefore, the high-quality reservoirs of the Yeli-Liangjiashan Formation and Fengshan Formation are mainly distributed at the paleokarst boundary (unconformity), and their distributions are planar.

From a regional perspective, micritic dolomite, micrite, and salt-rock are quickly formed in the granular beach environment, forming an impermeable layer between the beach facies; their primary pores are not developed, and atmospheric freshwater has difficulty penetrating [72–74]. Thus, only a thin surface cavity layer (surface karst zone) is formed in the surface layer. Karstification occurs during the infiltration of cracks, resulting in a lateral or longitudinal channel for local fluid migration [58]. Compared with that of granular beach facies dolomite, its reservoir performance is significantly lower, and it often forms a tight reservoir (Figure 13a). Due to the leaching effect of atmospheric freshwater, restricted platform limestone and limy dolomite are prone to develop vertically dissolved pores and caves. They are vertically connected with high-angle cracks, which can become excellent vertical fluid transport channels. When encountering impermeable layers, cracks

and pores with good reservoir properties can form [73]. Compared with those of granular dolomite, the porosity and permeability of grainy dolomite in an evaporation platform are better, but the order of the grains is relatively disordered [74]. When strata are exposed to denudation and subjected to the leaching of atmospheric freshwater, their developed karst patterns are also different due to the differences in their structural locations. In the higher terrain areas (karst highlands and karst slopes), the thickness of the vadose zone is relatively large. The vertical development of dissolved pores, solution caves, connected cracks, and sinkholes can form an excellent banded reservoir, which is affected by the underflow zone and boundary [75]. A layered dissolved pore zone and an underground river are developed in the lower part of the underflow zone. A good stratified reservoir can be formed. When the grainy dolomite is located in a relatively flat and low-lying area, the vertical flow and dissolution process of atmospheric freshwater occurs in the surface cracks of the grains over a short distance. Then, forward flow occurs in the grains to develop layered dissolved pores, and finally, a high-porosity reservoir can form.
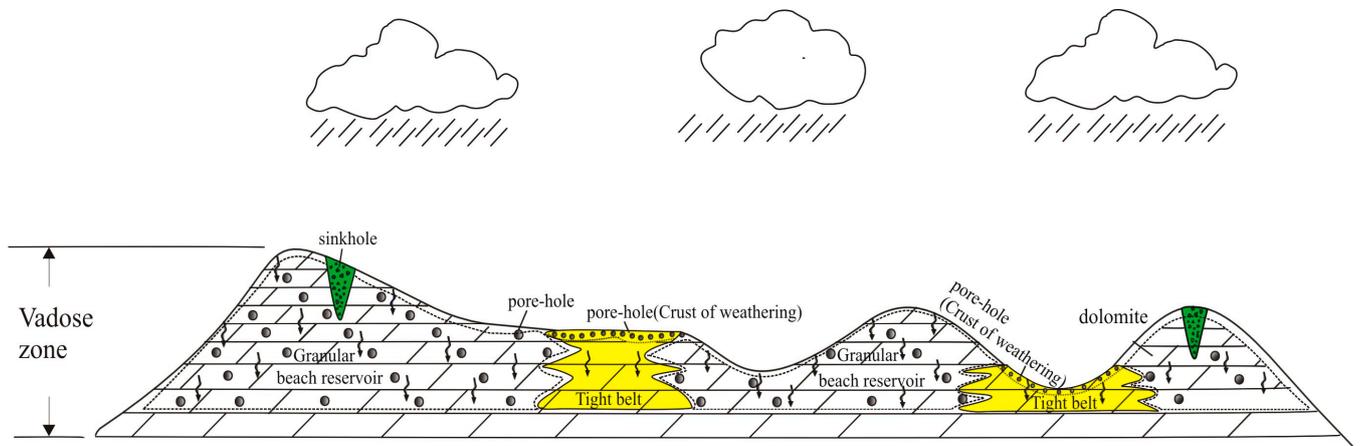
（a）Lateral heterogeneity is caused by the difference of reservoir performance between granular beaches
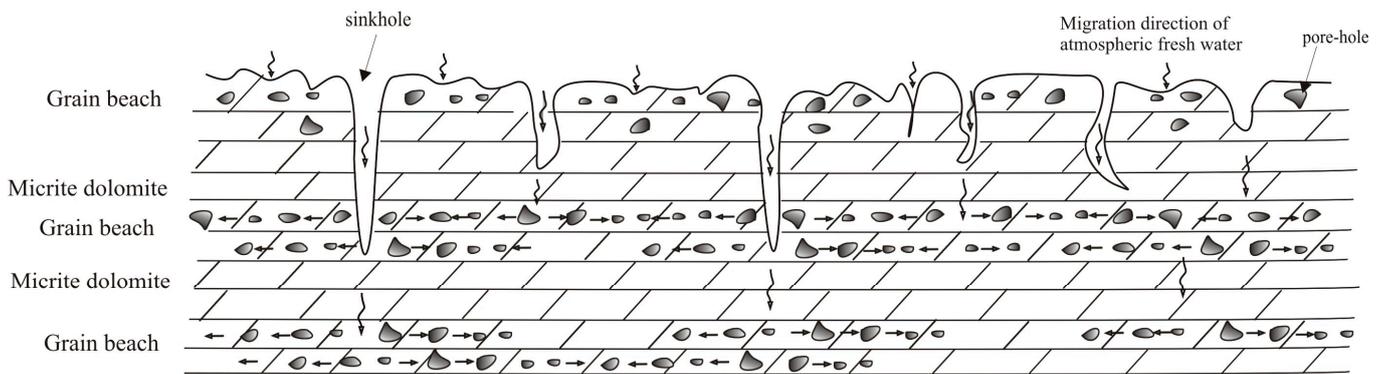
（b）The vertical flow of the vadose zone in the granular beach forms the solution channel and the solution cracks, and the lateral flow of atmospheric water in the underflow zone forms the layered dissolved pore zone

Figure 13. Huaiyuan period reservoir development model map of Yeli-Liangjiashan Formation and Fengshan Formation in Chengdao-Zhuanghai buried hill.

6. Conclusions

This study aimed to reveal the influence of supergene karstification on reservoir formation during the Huaiyuan Movement. The most important conclusions are as follows:

(1) Geological and geochemical data indicate that the Fengshan Formation and Yeli-Liangjiashan Formation were affected and controlled by the Huaiyuan Movement and have apparent vertical karst zonation. From top to bottom, the vadose zone and

the underflow zone can be delimited successively, the karst breccia is present in the two karst zones, and differences are present.

(2) There are apparent differences in the types of reservoir space combinations between the vadose and underflow zones. In the vadose zone, the dissolved pores, karst caves, and cracks formed by weathering solutions are present and are connected longitudinally. It is easy to develop a composite crack-cavity reservoir space. In contrast, in the underflow zone, layered dissolved pores and cracks are present, and it is easy to develop two types of reservoir spaces: cavity type and crack type.

(3) Primitive sedimentary microfacies, dolomitization, and supergene karstification controlled the Fengshan Formation and Yeli-Liangjiashan Formation reservoirs. Different sedimentary microfacies have apparent differences in the mode of karst development, development intensity, reservoir type, and reservoir physical properties. The reservoirs are mainly distributed along the paleokarst zone that formed in the Huaiyuan period, and the dolomite of the granular beach facies has the best reservoir physical properties, which are the features of surface distribution along the upper unconformity in the region.

(4) Limited by the progress of the current work, the data obtained, and the research methods, the longitudinal and transverse connectivity of the internal reservoir space of the unconformity structure has not been studied, and it is necessary to increase the logging data and seismic experiments to carry out this research. It is suggested that there are longitudinal and transverse migration channels in the unconformity affected by the Huaiyuan movement, and combined with faults formed by multi-stage tectonic movement, they form a network of fluid (oil and gas) transport systems. In the strata of the Jiyang Depression, a large number of source rocks are distributed in the Paleogene strata. Under mature hydrocarbon expulsion, the source rocks migrate continuously along the Paleogene sand body and reach the buried hill of the Lower Paleozoic. After that, the hydrocarbon-bearing fluid migrates and transports horizontally or vertically along the network transport system, forming hydrocarbon accumulations in the buried hill of the lower Paleozoic in the Jiyang Depression. Thus, a new network reservoir formation system is formed, which opens a new avenue for the exploration of the Jiyang Depression and provides a new research direction for the study of the area affected by the Huaiyuan movement in Bohai Bay Basin, China.

References

1. Fritz, R.D.; Wilson, J.L.; Yurewicz, D.A. *Paleokarst Related Hydrocarbon Reservoirs*; SEPM Society for Sedimentary Geology: Claremore, OK, USA, 1993.
2. Halbouty, M.T. *Giant Oil and Gas Fields of the 1990s: An Introduction*; American Association of Petroleum Geologists: Tulsa, OK, USA, 2003.

3.   Gu, Z.D.; Wang, Z.C.; Hu, S.Y.; Wang, H.; Yin, J.F.; Huang, P.H. Tectonic settings of global marine carbonate giant fields and exploration significance. *Nat. Gas Geosci.* **2012**, *23*, 106–118.

4.   Budd, D.A.; Saller, A.H.; Harris, P.M. Unconformities and porosity in carbonate strata. *AAPG Mem.* **1995**, *79*, 1183–1184.

5.   Clari, P.A.; Pierre, F.D.; Martire, L. Discontinuities in carbonate successions: Identification, interpretation and classification of some Italian examples. *Sediment. Geol.* **1995**, *100*, 97–121. [CrossRef]

6.   Akbar, M.; Vissapragada, B.; Alghamdi, A.H.; Allen, D.; Herron, M.; Carnegie, A.; Dutta, D.; Olesen, J.-R.; Logan, D.; Stief, D.; et al. A snapshot of carbonate reservoir evaluation. *Oilfield Rev.* **2000**, *12*, 20–21.

7.   Wang, B.; Al-Aasm, I.S. Karst-controlled diagenesis and reservoir development: Example from the Ordovician mainreservoir carbonate rocks on the eastern margin of the Ordos basin, China. *AAPG Bull.* **2002**, *86*, 1639–1658.

8.   Sattler, U.T.E.; Immenhauser, A.; Hillgärtner, H.; Esteban, M. Characterization, lateral variability and lateral extent of discontinuity surfaces on a carbonate platform (Barremian to Lower Aptian, Oman). *Sedimentology* **2005**, *52*, 339–361. [CrossRef]

9.   Craig, J.; Thurow, J.; Thusu, B.; Whitham, A.; Abutarruma, Y. *Global Neoproterozoic Petroleum Systems: The Emerging Potential in North Africa*; Geological Society London, Special Publications: London, UK, 2009; Volume 326, pp. 1–25.

10.   Su, J.; Zhang, S.C.; Yang, H.J.; Zhu, G.Y.; Chen, J.P.; Zhang, B. The control of carbonate effective reservoir by fault system and its reservoir-forming rule. *Acta Pet. Sin.* **2010**, *31*, 196–203.

11.   Chow, N.; Wendte, J. Palaeosols and palaeokarst beneath subaerial unconformities in an Upper Devonian isolated reef complex (Judy Creek), Swan Hills Formation, west-central Alberta, Canada. *Sedimentology* **2011**, *58*, 960–993. [CrossRef]

12.   Bhat, G.M.; Craig, J.; Hafiz, M.; Hakhoo, N.; Thurow, J.W.; Thusu, B.; Cozzi, A. *Geology and Hydrocarbon Potential of Neoproterozoic–Cambrian Basins in Asia: An Introduction*; Geological Society, London, Special Publications: London, UK, 2012; Volume 366, pp. 1–17.

13.   Bagni, F.L.; Bezerra, F.H.; Balsamo, F.; Maia, R.P.; Dall'Aglio, M. Karst dissolution along fracture corridors in an anticline hinge, Jandaíra Formation, Brazil: Implications for reservoir quality. *Mar. Pet. Geol.* **2020**, *115*, 104249. [CrossRef]

14.   Ji, Y.L.; Hu, G.M.; Zhang, S.W.; Zhao, J.Q. Mineralogical and geochemical methods in study of sedimentary sequence boundary. *Tongji Daxue Xuebao/J. Tongji Univ. (Nat. Sci.) (China)* **2004**, *32*, 455–460.

15.   Bai, B.; Zou, C.; Zhu, R.; Zhai, W.L.; Liu, L.H.; Dai, Z.C.; Mao, Z.G. Integrated identification of sequence boundaries through outcrop, natural gammaray spectral, rock geochemistry, logging and seismic: A case of upper Triassic Xujiahe formation, Sichuan Basin. *Nat. Gas Geosci.* **2010**, *21*, 78–86.

16.   Zhiqian, G.; Tailiang, F. Unconformities and their influence on lower Paleozoic petroleum reservoir development in the Tarim Basin. *J. Pet. Sci. Eng.* **2015**, *133*, 335–351. [CrossRef]

17.   Beckert, J.; Vandeginste, V.; John, C.M. Relationship between karstification and burial dolomitization in Permian platform carbonates (Lower Khuff—Oman). *Sediment. Geol.* **2016**, *342*, 165–179. [CrossRef]

18.   Vincent, S.J.; Guo, L.; Flecker, R.; BouDagher-Fadel, M.K.; Ellam, R.M.; Kandemir, R. Age constraints on intra-formational unconformities in Upper Jurassic-Lower Cretaceous carbonates in northeast Turkey; geodynamic and hydrocarbon implications. *Mar. Pet. Geol.* **2018**, *91*, 639–657. [CrossRef]

19.   Nadeau, O. Sources of fluids in Archean hydrothermal stockwork-disseminated gold deposits of Abitibi, Canada: Insights from Duquesne, Dolodau, Lac Shortt and Canadian Malartic. *Ore Geol. Rev.* **2019**, *111*, 102975. [CrossRef]

20.   Lyu, D.; Deng, Y.; Wang, H.; Zhang, F.; Ren, R.; Gao, Z.; Canfield, D.E. Using cyclostratigraphic evidence to define the unconformity caused by the Mesoproterozoic Qinyu Uplift in the North China Craton. *J. Asian Earth Sci.* **2021**, *206*, 104608. [CrossRef]

21.   James, N.P.; Choquette, P.W. (Eds.) *Paleokarst*; Springer Science & Business Media: Berlin/Heidelberg, Germany, 2012.

22.   Lucia, F.J. *Lower Paleozoic Cavern Development, Collapse, and Dolomitization, Franklin Mountains, El Paso, Texas*; American Association of Petroleum Geologists: Tulsa, OK, USA, 1995.

23.   Luczaj, J.A.; Harrison, W.B., III; Smith Williams, N. Fractured hydrothermal dolomite reservoirs in the Devonian Dundee Formation of the central Michigan Basin. *AAPG Bull.* **2006**, *90*, 1787–1801. [CrossRef]

24.   Tian, H.; Xiao, X.; Wilkins, R.W.; Tang, Y. New insights into the volume and pressure changes during the thermal cracking of oil to gas in reservoirs: Implications for the in-situ accumulation of gas cracked from oils. *AAPG Bull.* **2008**, *92*, 181–200. [CrossRef]

25.   Cao, J.W. *Study on the Distribution and Genetic Mechanism of Paleokarst in the Eastern Part of Lunnan Buried Mountain*; China University of Geosciences: Wuhan, China, 2019.

26.   Jiu, B.; Huang, W.; Mu, N.; Hao, R. Petrology, mineralogy and geochemistry of Ordovician rocks in the southwest of Tarim Basin, implications for genetic mechanism and evolution model of the hydrothermal reformed-paleokarst carbonate reservoir. *Mar. Pet. Geol.* **2022**, *140*, 105687. [CrossRef]

27.   Li, P.L.; Zhang, S.W.; Wang, Y.S. *Genesis, Accumulation and Exploration of Diverse Buried Hills: A Case Study of Jiyang Depression*; Petroleum Industry Press: Beijing, China, 2003.

28.   Song, G.Q.; Zhuo, Q.G.; Sun, L. Migration and accumulation model of Tertiary unconformity hydrocarbon reservoirs in Jiyang Depression. *Oil Gas Geol.* **2008**, *29*, 716–720+732.

29.   Sui, F.G.; Song, G.Q.; Zhao, L.Q.; Wang, X.J. Oil and gas transport mode and performance of unconformity in continental faulted basin of Jiyang Depression. *J. China Univ. Pet. (Nat. Sci. Ed.)* **2010**, *34*, 44–48.

30.   Ma, L.C. Discussion on genesis of lower Paleozoic insider-type reservoir in Jiyang Depression. *Spec. Reserv.* **2003**, *10*, 13–14+91.

31.   Lin, H.X. Karstification of lower Paleozoic buried hill reservoir in Zhuangxicheng Island area, Jiyang Depression. *J. Chengdu Univ. Technol. (Sci. Technol. Ed.)* **2004**, *42*, 490–497.

32. Song, D.N. Reunderstanding of Huaiyuan movement. *Geol. Shandong* **2001**, *17*, 19–23.
33. Li, X.B.; Wang, H.B.; Huang, J.P.; Zhang, C.L.; Zhang, Y.; Wang, Y.T.; Zhang, L.; Wang, J.; Liu, H.Q. Characteristics of Huaiyuan movement unconformity in Ordos Basin and its significance for oil and gas exploration. *Oil Gas Geol.* **2021**, *42*, 1043–1055.
34. Zhang, M.; Wu, Z.P.; Huang, Z.; Zhang, B.; Zhang, F.P.; Miao, Y.Z. Development law and genetic type division of buried hill in Jiyang Depression, Bohai Bay Basin. *Earth Sci.* **2023**, *48*, 488–502.
35. Wang, Z.; Zhang, K.; Cheng, Y.; Wu, Q. Identification and evaluation of fault-fracture reservoirs in buried hills of the Lower Paleozoic, Chengdao area, China. *Energy Geosci.* **2023**, *4*, 100183. [CrossRef]
36. Jing, A.Y. Fault characteristics and reservoir-controlling effect of Lower Paleozoic buried hill in Chengdao area of Jiyang Depression. *Sci. Technol. Eng.* **2020**, *20*, 6011–6017.
37. Ma, S.; Wang, Y.S.; Wang, X.J.; Jing, A.Y. Development characteristics and genetic mechanism of Lower Paleozoic buried hill insider dolomite reservoir in Jiyang Depression. *Geol. Rev.* **2023**, *69*, 279–280.
38. Zhang, Y.F.; Wang, Q.C. Isotopic characteristics and significance of calcite C and O in Ordovician carbonate rocks and fracture-cavity filling in Jiyang Depression. *Chin. J. Geol.* **2007**, *42*, 570–578.
39. Osleger, D.; Read, J.F. Relation of eustasy to stacking patterns of meter-scale carbonate cycles, Late Cambrian, USA. *J. Sediment. Res.* **1991**, *61*, 1225–1252.
40. Liu, B.; Wang, Y.H.; Qian, X.L. Genesis of two Ordovician unconformities and prediction of related regional reservoirs in North China. *Acta Sedimentol.* **1997**, *15*, 25–30.
41. Mei, M.X.; Ma, Y.S. Late Cambrian sequence stratigraphy of North China Platform and its correlation with sea level change of North American platform. *Sediment. Tethys Geol.* **2003**, *23*, 14–26.
42. Cross, N.E.; van Veen, L.J.; Al-Enezi, A.; Singh, S.; van Beusekom, G. Seismic geomorphology of karst in Cretaceous to Early Cenozoic carbonates of North Kuwait. *Mar. Pet. Geol.* **2021**, *128*, 104947. [CrossRef]
43. Li, Y.; Jin, Q.; Zhong, J.H.; Zou, S.Z. Characteristics of Ordovician karst zonation and fissure cavity structure in Tahe Oilfield. *Acta Pet. Sin.* **2016**, *37*, 289–298.
44. Zhang, Q.Y.; Liang, B.; Cao, J.W.; Dan, Y.; Li, J.R.; Chen, L.X. Pre-carboniferous paleo-karst microgeomorphology and karst development model in east Lungu area, Tarim Basin. *Mar. Pet. Geol.* **2017**, *22*, 30–36.
45. Veizer, J.; Ala, D.; Azmy, K.; Bruckschen, P.; Buhl, D.; Bruhn, F.; Strauss, H. $^{87}Sr/^{86}Sr$, $\delta^{13}C$ and $\delta^{18}O$ evolution of Phanerozoic seawater. *Chem. Geol.* **1999**, *161*, 59–88. [CrossRef]
46. Denison, R.E.; Koepnick, R.B.; Burke, W.H.; Hetherington, E.A. Construction of the Cambrian and Ordovician seawater 87Sr/86Sr curve. *Chem. Geol.* **1998**, *152*, 325–340. [CrossRef]
47. Clayton, R.N.; Degens, E.T. Use of carbon isotope analyses of carbonates for differentiating fresh-water and marine sediments. *AAPG Bull.* **1959**, *43*, 890–897.
48. Meng, Q.Q.; Zhu, D.Y.; Hu, W.X.; Jin, Z.J. Dissolution-filling mechanism of atmospheric precipitation controlled by both thermodynamics and kinetics. *Sci. China Earth Sci.* **2013**, *56*, 2150–2159. [CrossRef]
49. Jones, B. Diagenetic processes associated with unconformities in carbonate successions on isolated oceanic islands: Case study of the Pliocene to Pleistocene sequence, Little Cayman, British West Indies. *Sediment. Geol.* **2019**, *386*, 9–30. [CrossRef]
50. Bagni, F.L.; Erthal, M.M.; Tonietto, S.N.; Maia, R.P.; Bezerra, F.H.; Balsamo, F.; Fonseca, J.P.T. Karstified layers and caves formed by superposed epigenic dissolution along subaerial unconformities in carbonate rocks–Impact on reservoir-scale permeability. *Mar. Pet. Geol.* **2022**, *138*, 105523. [CrossRef]
51. Xiong, Y.; Tan, X.; Zhong, S.; Xiao, D.; Wang, B.; Yang, M.; Cao, J. Dynamic paleokarst geochemistry within 130 Myr in the Middle Ordovician Shanganning carbonate platform, North China. *Palaeogeogr. Palaeoclimatol. Palaeoecol.* **2022**, *591*, 110879. [CrossRef]
52. Esrafili-Dizaji, B.; Rahimpour-Bonab, H. Effects of depositional and diagenetic characteristics on carbonate reservoir quality: A case study from the South Pars gas field in the Persian Gulf. *Petrol. Geosci.* **2009**, *15*, 325–344. [CrossRef]
53. Mehrabi, H.; Rahimpour-Bonab, H.; Hajikazemi, E.; Jamalian, A. Controls on depositional facies in Upper Cretaceous carbonate reservoirs in the Zagros area and the Persian Gulf, Iran. *Facies* **2015**, *61*, 23. [CrossRef]
54. Ma, C.F.; Huang, W.J.; Du, Z.L.; Han, W.Z.; Zhan, Y.; Shi, Z.N.; Zhou, J.; Song, M.Y. Lithofacies classification scheme of continental lacustrine shale and its significance: A case study of the second member of Kongdian Formation in Cangdong Sag. *J. Cent. South Univ. Nat. Sci. Ed.* **2022**, *53*, 3287–3300.
55. Vandeginste, V.; Swennen, R.; Reed, M.H.; Ellam, R.M.; Osadetz, K.; Roure, F. Host rock dolomitization and secondary porosity development in the upper Devonian Cairn Formation of the Fairholme carbonate complex (south-west Alberta, Canadian Rockies): Diagenesis and geochemical modelling. *Sedimentology* **2009**, *56*, 2044–2060. [CrossRef]
56. Adams, J.E.; Rhodes, M.L. Dolomitization by seepage refluxion. *AAPG Bull.* **1961**, *44*, 1912–1920.
57. Skall, H. The paleoenvironment of the Pine Point lead-zinc district. *Econ. Geol.* **1975**, *70*, 22–47. [CrossRef]
58. Lucia, F.J.; Major, R.P. Porosity evolution through hypersaline reflux dolomitization. In *Dolomites: A Volume in Honour of Dolomieu*; John Wiley & Sons, Inc.: Hoboken, NJ, USA, 1994; pp. 325–341.
59. Meng, M.; Ge, H.; Shen, Y.; Ji, W.; Li, Z. Insight into water occurrence and pore size distribution by nuclear magnetic resonance in marine shale reservoirs, southern China. *Energy Fuels* **2023**, *37*, 319–327. [CrossRef]
60. Sullivan, E.C.; Marfurt, K.J.; Lacazette, A.; Ammerman, M. Application of new seismic attributes to collapse chimneys in the Fort Worth Basin. *Geophysics* **2006**, *71*, B111–B119. [CrossRef]

61. Zhao, W.; Shen, A.; Qiao, Z.; Zheng, J.; Wang, X. Carbonate karst reservoirs of the Tarim Basin, northwest China: Types, features, origins, and implications for hydrocarbon exploration. *Interpretation* **2014**, *2*, SF65–SF90. [CrossRef]
62. Chopra, S.; Marfurt, K.J. Seismic attributes for stratigraphic feature characterization. In *SEG Technical Program Expanded Abstracts 2008*; Society of Exploration Geophysicists: Houston, TX, USA, 2008; pp. 1590–1594.
63. Ma, Y.; Zhang, S.; Guo, T.; Zhu, G.; Cai, X.; Li, M. Petroleum geology of the Puguang sour gas field in the Sichuan Basin, SW China. *Mar. Pet. Geol.* **2008**, *25*, 357–370. [CrossRef]
64. Meng, M.; Ge, H.; Shen, Y.; Ji, W.; Wang, Q. Rock fabric of tight sandstone and its influence on irreducible water saturation in Eastern Ordos Basin. *Energy Fuels* **2023**, *37*, 3685–3696. [CrossRef]
65. Al-Aasm, I. Origin and characterization of hydrothermal dolomite in the Western Canada Sedimentary Basin. *J. Geochem. Explor.* **2003**, *78*, 9–15. [CrossRef]
66. Smith, L.B., Jr. Origin and reservoir characteristics of Upper Ordovician Trenton–Black River hydrothermal dolomite reservoirs in New York. *AAPG Bull.* **2006**, *90*, 1691–1718. [CrossRef]
67. Chen, L.; Zhang, H.; Cai, Z.; Cong, F.; Huang, S.; Tang, P. Characteristics and formation mechanisms of the unconformity-related paleokarst reservoirs in the Upper Sinian, Northwestern Tarim Basin, China. *Mar. Pet. Geol.* **2020**, *120*, 104559. [CrossRef]
68. Flügel, E.; Munnecke, A. *Microfacies of Carbonate Rocks: Analysis, Interpretation and Application*; Springer: Berlin, Germany, 2010; Volume 976, p. 2004.
69. Murray, R.C. Origin of porosity in carbonate rocks. *J. Sediment. Res.* **1960**, *30*, 59–84. [CrossRef]
70. Lucia, F.J.; Kerans, C.; Jennings, J.W., Jr. Carbonate reservoir characterization. *J. Pet. Technol.* **2003**, *55*, 70–72. [CrossRef]
71. Ford, D.; Williams, P.D. *Karst Hydrogeology and Geomorphology*; John Wiley & Sons: Hoboken, NJ, USA, 2007.
72. La Bruna, V.; Bezerra, F.H.; Souza, V.H.; Maia, R.P.; Auler, A.S.; Araujo, R.E.; Sousa, M.O. High-permeability zones in folded and faulted silicified carbonate rocks–implications for karstified carbonate reservoirs. *Mar. Pet. Geol.* **2021**, *128*, 105046. [CrossRef]
73. Scholle, P.A.; Bebout, D.G.; Moore, C.H. *Carbonate Depositional Enviroments*; American Association of Petroleum Geologists: Tulsa, OK, USA, 1983.
74. Meng, M.; Zhang, Y.; Yuan, B.; Li, Z.; Zhang, Y. Imbibition behavior of oil-saturated rock: Implications for enhanced oil recovery in unconventional reservoirs. *Energy Fuels* **2023**, *37*, 13759–13768. [CrossRef]
75. He, J.; Fang, S.; Hou, F.; Yan, R.; Zhao, Z.; Yao, J.; Tang, X.; Wu, G. Vertical zonation of weathered crust ancient karst and reservoir evaluation and prediction—A case study of M55–M51 sub-members of Majiagou Formation in gas fields, central Ordos Basin, NW China. *Pet. Explor. Dev.* **2013**, *40*, 572–581.